

ESTIMATION OF PEAK HORIZONTAL
GROUND ACCELERATION
AT SAN ONOFRE
NUCLEAR GENERATING STATION

Submitted to:

Mr. H. Gene Hawkins
Southern California Edison
P.O. Box 800
Rosemead, California 91770

February 19, 1982

 TERA CORPORATION

2150 Shattuck Avenue
Berkeley, California 94704
415-845-5200

Berkeley, California
Dallas, Texas
Bethesda, Maryland
Baton Rouge, Louisiana
Del Mar, California
New York, New York
San Antonio, Texas
Denver, Colorado
Los Angeles, California

8204200350 820415
PDR ADOCK 05000206
P PDR

REGULATORY DOCKET FILE COPY

TABLE OF CONTENTS

<u>Section</u>	<u>Page</u>
Summary	1
Introduction	1
Near Source Data Base	3
Ground Motion Model	9
Ground Motion Characteristics	21
Sensitivity Studies	28
Discussion	42
Conclusions	51
References	53
Appendix - Strong Motion Data	57

LIST OF TABLES

Table

- 1 Earthquake Data
- 2 Geological Classification Scheme
- 3 Distribution of Earthquake Recordings
- 4 Distribution of Recordings with Respect to Geology and Fault Type
- 5 Near-field Properties of the Four Ground-Motion Models Containing the Function $C(M)$
- 6 Sensitivity Results for Variations in Functional Form
- 7 Sensitivity Results for Variations in Far-Field Attenuation Rate for the Constrained Model
- 8 A Summary of Class I Data Excluded from Analysis of PGA
- 9 A Summary of Class II Data Excluded from Analysis of PGA
- 10 Distance Saturation Characteristics of Near-Source Acceleration
- 11 Magnitude Saturation Characteristics of Near-Source Acceleration

LIST OF FIGURES

Figure

- 1 Distribution of Strong-Motion Recordings with Respect to Magnitude and Distance
- 2 The Unconstrained Ground Motion Model (Eq. 3) Plotted as a Function of Distances of Magnitudes 5.0 to 8.0
- 3 The Unconstrained Ground Motion Model (Eq. 3) Plotted as a Function of Magnitude for Fault Distances 0 to 50 Kilometers
- 4 A Plot of Residuals as a Function of Fault Distance - Unconstrained Regression Analysis (Eq. 3)
- 5 A Comparison of Observed Versus Predicted values Plotted Versus Fault Distance - Unconstrained Ground Motion Model (Eq. 3)
- 6 A Comparison of Observed Versus Predicted Values Plotted Versus Magnitude - Unconstrained Ground Motion Model (Eq. 3)
- 7 A Plot of Residuals as a Function of Fault Distance - Constrained Ground Motion Model (Eq. 5)
- 8 A Comparison of the Unconstrained and Constrained Ground Motion Model
- 9 Normal Probability Plot and Distribution of Residuals
- 10 A Comparison of Observed Versus Predicted Values for Excluded Class I Data with Unknown Fault Distance
- 11 A Comparison of Observed Versus Predicted Values for Excluded Class II Data with Unknown Fault Distance
- 12 Observed and Predicted Mean Horizontal Peak Acceleration for the October 15, 1979, Imperial Valley Earthquake
- 13 The Unconstrained Ground Motion Model Compared with the Attenuation Relationship Developed by Joyner and Boore (1981)

SUMMARY

Strong-motion data recorded within 50 kilometers of the rupture zone were used to study near-source scaling characteristics of horizontal peak ground acceleration for the purpose of estimating peak accelerations at San Onofre Nuclear Generating Station (SONGS) associated with an M_s 7.0 earthquake occurring eight kilometers offshore on the Offshore Zone of Deformation (OZD). The data base consisted of 229 horizontal components of peak acceleration recorded from 27 worldwide earthquakes of magnitudes 5.0 to 7.7, including the October 15, 1979, Imperial Valley earthquake. These data were found to be adequately represented by the functional relationship

$$PGA = a \exp(bM) \left[R + C(M) \right]^{-d}$$

where PGA represents the mean of the two horizontal components of peak acceleration, M is Richter magnitude, and R is shortest distance to the fault rupture zone. Peak acceleration was found to be lognormally distributed with an 84th-percentile estimate 45-percent larger than the median estimate.

Two ground motion models were developed and tested in this study. The first was developed from a regression analysis that statistically established all the coefficients in the above relationship. In a second analysis, certain near-field and far-field constraints were applied in order to accommodate observed and analytical characteristics of strong ground motion. The regression analysis statistically confirmed the results of earthquake simulation studies that have indicated a tendency for peak acceleration to become independent of magnitude and distance in the near field.

In order to test the appropriateness of the ground motion models developed in this study for estimating peak accelerations at SONGS, an analysis of residuals was used to investigate the behavior of peak acceleration with respect to various earthquake, site, and recording parameters. The more significant findings were (1) a similarity in the level of acceleration recorded on soil and rock, (2) larger than average accelerations recorded at sites located on shallow soils or in areas of steep topography, (3) larger than average accelerations associated with earthquakes having reverse fault mechanisms, and (4) lower than average accelerations recorded in large embedded structures.

The results of sensitivity studies on the predictions of PGA for M_s 7.0 at eight kilometers have indicated that the ground motion models developed in this study are appropriate for estimating peak acceleration at SONGS, these predictions being 0.33 g and 0.48 g for the median and 84th-percentile, respectively. We found these predictions to be very stable with respect to reasonable model and parameter variations.

INTRODUCTION

The recent expansion of strong-motion networks throughout the world has been responsible for the recording of several significant accelerograms in the near-source region of moderate-to-large earthquakes, an area where data have been severely lacking in the past. Three significant events which have occurred within the past five years are the 1976 Gazli, U.S.S.R., (M_s 7.0), the 1978 Tabas,

Iran, (M_s 7.7) and the 1979 Imperial Valley, U.S.A., (M_s 6.9) earthquakes, each producing accelerograms within ten kilometers of the fault.

These and other recent near-source recordings together with selected near-source data recorded as early as 1933 were used to analyze the behavior of peak horizontal acceleration (PGA) near the causative fault. The goal was to make PGA predictions at these distances as generally reliable as far-field estimates. The study was restricted to the near-source region of earthquakes of magnitude 5.0 or greater to eliminate the small accelerations generally considered to be of little importance in earthquake engineering. This restriction substantially reduced the uncertainty in the analyses and enhanced the statistical significance of the results.

Due to the paucity of near-source data for large earthquakes, the study was not restricted to accelerations recorded in western North America. We acknowledge that the tectonics and recording practices of other countries may be substantially different from those in the western United States, but these possible differences are far outweighed by the important contribution these foreign data make to understanding the behavior of near-source ground motion.

Several factors have minimized the potential bias of the foreign data used in the analyses. First, the restriction to the near-source region has made differences in anelastic attenuation negligible compared to the inherent scatter from other factors. In addition, the foreign data used in this investigation come from events occurring along tectonic plate boundaries which are generally similar to the interplate earthquakes of western North America. Deep subduction events were excluded because of the substantial difference in travel paths and stress conditions compared to the shallow events used in this study. All the foreign data were recorded on instruments having dynamic characteristics similar to those commonly used in the United States to avoid a possible instrument bias for these recordings as is systematically observed for the SMAC strong-motion accelerograph generally used in Japan.

The data base used in the analyses was assembled using criteria designed to select only consistent and quality data in the range of magnitudes and distances of interest for most design applications. The data base consisted of 27 earthquakes representing 229 horizontal components (116 records) of peak ground acceleration recorded at distances from the rupture zone of less than 30 or 50 kilometers, dependent on magnitude. These data were weighted, by earthquake, within several distance intervals to control the effects of well-recorded events such as the 1979 Imperial Valley and the 1971 San Fernando earthquakes.

Two ground motion models were developed and tested in this study. The first was an empirical relationship whose coefficients were determined based solely on regression analysis. Because of the limited amount of data within three to five kilometers of the rupture zone and because our restriction to the near-source region excluded data beyond 50 kilometers, a second ground motion model having specified near-field and far-field properties was developed and compared to the empirical model. As a result, two boundary conditions were applied in the second analysis. First, the far-field attenuation of PGA was constrained to $R^{-1.75}$ based upon the studies of other investigators, and second, PGA at the

fault rupture surface was constrained to a constant value, independent of magnitude, consistent with the physics of the earthquake rupture process.

NEAR-SOURCE DATA BASE

The general data base consists of peak acceleration data recorded in the near-source region of a set of worldwide earthquakes with shallow rupture. It represents available published peak acceleration data recorded in the United States through at least March 1979 that meet the following criteria:

- (1) Earthquakes for which either epicenters were determined with an accuracy of 5 kilometers or less, or an accurate estimate of the closest distance to the fault rupture surface was known;
- (2) Earthquake magnitude determinations were accurate to within 0.3 units;
- (3) Source-to-site distances were within 20, 30, and 50 kilometers for magnitudes less than 4.75, between 4.75 and 6.25, and greater than 6.25, respectively;
- (4) Earthquake hypocenters or rupture zones were within 25 kilometers of the ground surface;
- (5) Accelerograms had a PGA of at least 0.02 g for one component which triggered early enough in the record to capture the strong phase of shaking; and
- (6) Accelerograms were recorded on instruments either in the free field, on the abutments of dams or bridges, in the lowest basement of buildings, or on the ground level of structures without basements.

The data base was developed without any restriction on either the age of the record, the type of recording instrument, the recording site geology, the tectonic province of the earthquake, the earthquake fault type, or the size of the earthquake.

Several significant earthquakes which occurred either outside the United States or since March 1979 and which also met the selection criteria outlined above were included. They were: the August 6, 1979 Coyote Lake (M_L 5.9) and October 15, 1979 Imperial Valley (M_S 6.9) earthquakes in California; the December 10, 1967 Koyana, India, earthquake (M_S 6.5); the December 23, 1972 Managua, Nicaragua, earthquake (M_S 6.2); the October 3, 1974 Lima, Peru, earthquake (M_S 7.6); the May 17, 1976 Gazli, USSR, earthquake (M_S 7.0); and the September 16, 1978 Tabas, Iran, earthquake (M_S 7.7).

Various criteria were applied to the near-source data base in order to select a subset appropriate for the analysis of peak acceleration for moderate-to-large

magnitude earthquakes. The application of these criteria resulted in the selection of 229 horizontal components (116 recordings) of PGA from 27 earthquakes of magnitude 5.0 and greater. A list of these events appears in Table 1. The peak acceleration values, distances and geologic classification for the strong-motion stations are tabulated in the appendix. Figure 1 gives the distribution of recordings with respect to magnitude and distance. The correlation of these two parameters was found to be only six percent. A description of the selection criteria as well as definitions of important parameters of this selected data base are given below.

Peak Acceleration

Peak accelerations scaled from digitized, unprocessed accelerograms* were selected when available, otherwise values were scaled from the original accelerograms. Peak accelerations from fully processed accelerograms were not used because they are generally smaller than those scaled from either the digitized unprocessed or original accelerograms due to the 0.02 second decimation and frequency band-limited filtering of the records. The mean of the two horizontal peak values from an individual recording was used in the analysis because it was found to be a more stable peak acceleration parameter than either the single components taken separately or both components taken together. When only a single horizontal component was available, it was used in lieu of the mean value. The maximum of the two horizontal peak values used by some investigators (e.g., Boore et al., 1980) was found to be on the average 13-percent larger than the mean.

Magnitude

The study was restricted to earthquakes of magnitude 5.0 or greater because they are of greatest concern for most design applications. A magnitude scale which we will refer to as M in this paper was chosen to be generally consistent with both the moment-magnitude scale of Hanks and Kanamori (1979) and the Richter magnitude scale (as interpreted by Nuttli, 1979). It was defined as surface-wave magnitude (M_s) when both local magnitude (M_L) and surface wave magnitude were greater than or equal to 6.0, and it was defined as local magnitude when both magnitudes were below this value. Where M_s or M_L was not available, an appropriate value was estimated based upon empirical relationships among magnitude scales. The 1967 Fairbanks, Alaska, earthquake was the only selected event requiring such a conversion.

The use of M_s for the larger earthquakes not only served as a uniform basis for characterizing the magnitude of worldwide events, but also avoided the saturation effects that have been observed for the M_L and m_b scales (Chinnery, 1978; Kanamori, 1979). Moment magnitude, a scale designed to overcome the deficiencies caused by saturation of the conventional magnitude scales, was not

* This refers to the first stage in the routine processing of accelerograms in which the record is digitized and baseline corrected. Unequal digitization intervals are used to preserve the true value of the peaks recorded by the accelerograph.

TABLE I
EARTHQUAKE DATA

Earthquake Name	Date Yr-Mo-Day	Magnitude* (M)	Fault Type	No. of Recordings
Long Beach	33-03-11	6.2	Strike-Slip	3
Helena, Montana	35-10-31	5.5	Normal	1
Imperial Valley	40-05-19	7.1	Strike-Slip	1
Santa Barbara	41-07-01	5.9	Reverse	1
Kern County	52-07-21	7.7	Oblique	1
Daly City	57-03-22	5.3	Strike-Slip	5
Parkfield	66-06-28	6.0	Strike-Slip	4
Fairbanks, Alaska	67-06-21	5.7	Strike-Slip	1
Koyna, India	67-12-10	6.5	Strike-Slip	1
Borrego Mtn.	68-04-09	6.7	Strike-Slip	1
Lytle Creek	70-09-12	5.4	Strike-Slip	4
San Fernando	71-02-09	6.6	Reverse	24
Bear Valley	72-02-24	5.1	Strike-Slip	1
Sitka, Alaska	72-07-30	7.6	Oblique	1
Managua	72-12-23	6.2	Strike-Slip	1
Point Mugu	73-02-21	5.9	Reverse	1
Lima, Peru	74-10-03	7.6	Reverse	2
Hollister	74-11-28	5.1	Strike-Slip	3
Oroville	75-08-01	5.7	Normal	4
Kalapana, Hawaii	75-11-29	7.1	Reverse	2
Gazli, USSR	76-05-17	7.0	Reverse	1
Santa Barbara	78-08-13	5.7	Reverse	6
Tabas, Iran	78-09-16	7.7	Reverse	1
Bishop	78-10-04	5.8	Strike-Slip	4
Malibu	79-01-01	5.0	Reverse	3
St. Elias, Alaska	79-02-28	7.2	Reverse	1
Coyote Lake	79-08-06	5.9	Strike-Slip	9
Imperial Valley	79-10-15	6.9	Strike-Slip	31

* Magnitude (M) was selected to be consistent with the moment-magnitude scale (see text):

$M = M_s$ for magnitudes equal to 6.0 or greater
 $M = M_L$ for magnitudes less than 6.0

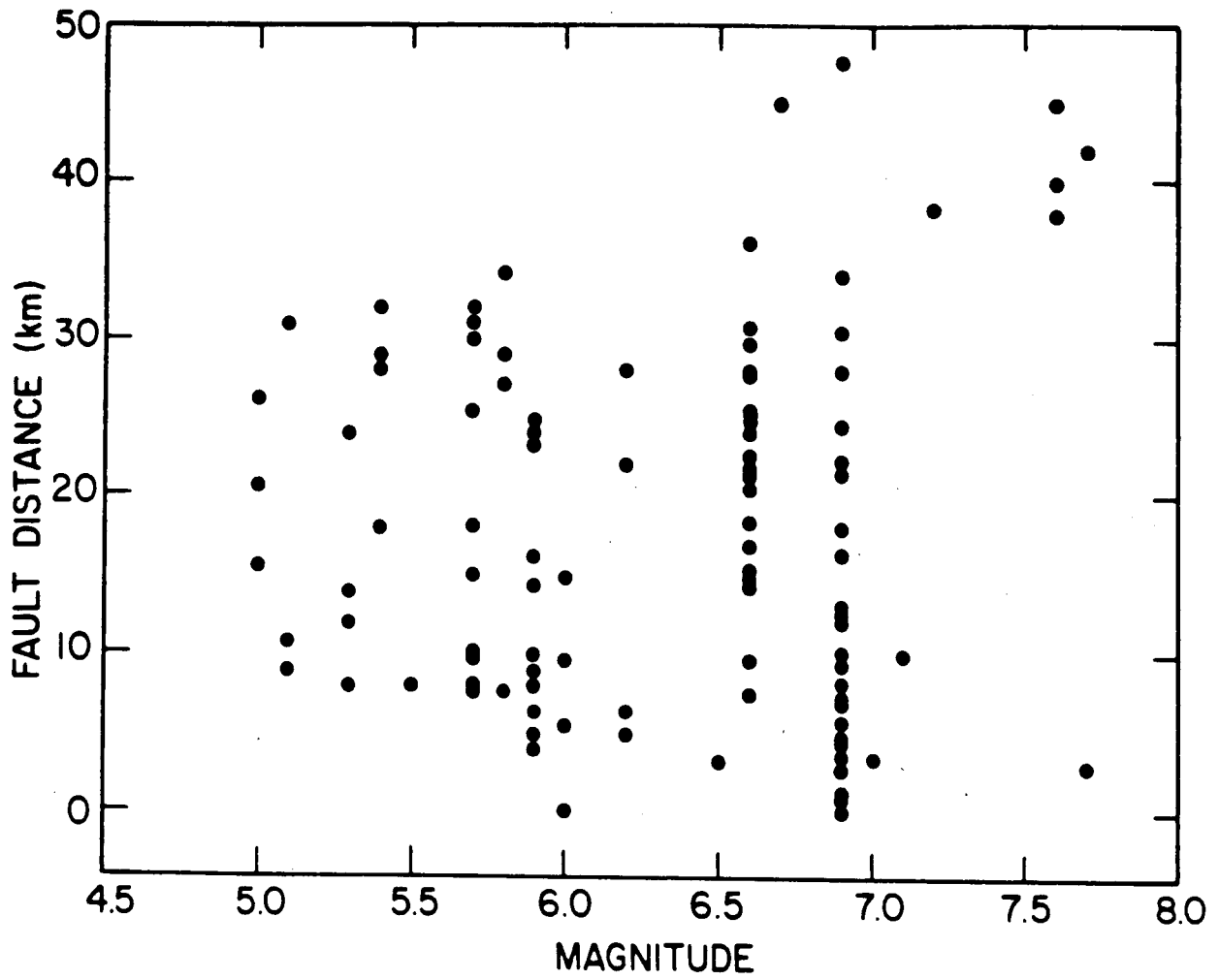


Figure 1. The distribution of strong-motion recordings with respect to magnitude and distance.

used because it was unavailable for many of the events used in this study and in many cases was less reliably determined than either M_L or M_S .

The actual agreement between our selected magnitude M and the moment-magnitude scale was tested by a comparative analysis. For the 18 events in the selected data base for which moment magnitudes were available, the average difference between the two scales was less than 0.2 units, with only two events (1974 Lima, Peru, and 1979 Imperial Valley) deviating by more than 0.3 units. The selected magnitudes were found to be quite insensitive to the actual value chosen as the division point between the choice of M_L or M_S . Of the few values of M that changed when this division point was varied from 5.5 to 6.5, the average variation in the selected magnitude was less than 0.2 units. These variations may be compared with a standard deviation of about 0.25 units for most reported magnitude values.

Source-To-Site Distance

Peak acceleration data were restricted to recording stations for which an accurate estimate of the shortest distance between the station and the fault rupture surface was available or could be determined. We found this distance, hereafter referred to as fault distance, to be statistically superior to either epicentral or hypocentral distance in representing the near-source attenuation characteristics of PGA. Closest distance to the fault rupture is believed to represent a more physically consistent and meaningful definition of distance for earthquakes having extensive rupture zones. These distances were computed from either the surface expression of faulting or the distribution of aftershocks. Consistent with the restriction to the near-source region, data were selected if distances were within 30 kilometers for $M \leq 6.25$ and within 50 kilometers for $M > 6.25$.

Site Geology

Peak accelerations from a wide range of site conditions were included in the analysis so that statistical trends in PGA between various geological classifications could be examined. A description of the classification scheme is found in Table 2. Based on results presented later in this paper, stations known to be situated at sites underlain by shallow soil deposits or extremely soft soils were not included in the final analysis. Statistical analysis has shown that the accelerations recorded at these sites are significantly different from those recorded at the other site conditions.

The Pacoima Dam record of the San Fernando earthquake was specifically excluded from the analysis for several reasons. First, the site experienced extreme topographic amplification (Boore, 1973; Mickey, et al., 1973). Second, the large gradation in wave propagation velocities and the low material damping in the upper 30 meters of rock (Duke et al., 1971) created a condition of extreme high-frequency resonance, thus placing the site in a category similar to shallow soil deposits. Third, there is evidence to suggest that the east-west response of the dam significantly amplified the $S74^{\circ}W$ component of the recorded motion (Mickey, et al., 1973; Reimer, et al., 1973).

TABLE 2
GEOLOGICAL CLASSIFICATION SCHEME

Site Geology	Description	Classification
Recent Alluvium	Holocene Age soil deposits with rock ≥ 10 m deep	A
Pleistocene Deposits	Pleistocene Age soil deposits with rock ≥ 10 m deep	B
Soft Rock	Sedimentary rock, soft volcanics and soft metasedimentary rock	C
Hard Rock	Crystalline rock, hard volcanics and hard metasedimentary rock	D
Shallow Soil Deposits	Holocene or Pleistocene Age soil deposits < 10 m deep overlying Soft or Hard Rock	E
Soft Soil Deposits	Extremely soft or loose Holocene Age soils such as beach sand or recent floodplain, lake, swamp, estuarine, and delta deposits.	F

Instrument Location

In order to assess the effects of the size and embedment of structures on recorded ground motion, peak acceleration data recorded on ground-level and basement-level instruments were selected for analysis. Ground-level instruments included those located on the ground level of buildings without basements, those housed within small shelters in the free field, and a few instruments located near the abutments of dams and bridges. Although the Koyana Dam record was actually located in the lower gallery within the dam, this recording was used in the analysis since it was believed to be representative of the motion at the base of the dam (Krishna et al., 1969).

In order to minimize possible bias associated with the large number of accelerations recorded during the 1971 San Fernando earthquake, we have used the San Fernando data reported by Boore et al. (1980). The criteria they applied lead to the selection of only a few stations from densely instrumented locations, such as downtown Los Angeles, resulting in a reasonable distribution of site types, distances, and instrument locations.

GROUND MOTION MODEL

The mathematical relationship used for modeling the scaling characteristics of near-source peak acceleration is expressed by the following equation:

$$PGA = a \exp(bM) [R + C(M)]^{-d} \quad (1)$$

where PGA is peak ground acceleration, R is fault distance and M is magnitude. This functional form was selected because, when used with regression analyses, it is capable of modeling possible nonlinear magnitude and distance scaling effects in the near field that may be supported by the data while incorporating the important features of other empirical relationships. The far-field properties of this relationship are characterized by the coefficient \underline{b} which controls magnitude scaling, and the coefficient \underline{d} which controls the geometrical attenuation rate.

The parameter C(M) modulates PGA attenuation at distances close to the fault where little geometrical attenuation is expected (Hadley and Helmberger, 1980). The distance at which the transition from far-field to near-field attenuation occurs is probably proportional to the size of the fault rupture zone, especially fault length for the larger shallow-focus events. Since fault rupture dimensions scale exponentially with magnitude, it would be expected that C(M) also scales exponentially with magnitude, as suggested by Esteva (1970). Therefore, the following relationship was used to model C(M):

$$C(M) = c_1 \exp(c_2 M) \quad (2)$$

Weighting Scheme

Weights were assigned to each recording to control the influence of the well-recorded earthquakes in the data base. It was thought that these weights should

depend on distance in order to account for the added information on attenuation represented by data from a single earthquake that are well-distributed with respect to distance. Of special concern were the 1971 San Fernando earthquake (24 recordings) and the 1979 Imperial Valley earthquake (31 recordings) which, combined, represent 48 percent of the acceleration data used in this study.

Seven weighting schemes were considered. At the one extreme was an unweighted analysis in which each recording carried an equal weight. In this case, well-recorded earthquakes have their greatest influence. For example, under this scheme, the 1979 Imperial Valley earthquake would have a weight of 27 percent (31 of 116 recordings) whereas the 1978 Tabas event would have a weight of 0.9 percent (1 of 116 recordings). At the other extreme was a weighting-by-earthquake scheme in which each earthquake carried an equal weight in the analysis. Here, well-recorded earthquakes have their least influence in the regressions with, for example, the Imperial Valley and Tabas events each having a weight of about four percent. The five other schemes used a number of distance intervals or bins in determining the weights, with earthquakes being weighted equally within each interval. These included nine-, eight-, seven-, five- and three-bin schemes.

Neither of the two extreme cases was considered to be a reasonable representation of the data. The unweighted case was found to place entirely too much emphasis on the well-recorded data at the expense of significant, singly-recorded events. For instance, Campbell (1980) found this scheme to give results identical to those obtained by removing the large magnitude non-North American events (1976 Gazli, 1978 Tabas, 1974 Lima and 1967 Koyna earthquakes) whose contribution to the magnitude scaling of PGA, especially in the near field, is significant but whose contribution to the data base is only five recordings. On the other hand, weighting-by-earthquake gives the same weight to an event having one recording as it does to a multiply-recorded event. Yet, the singly-recorded event provides no direct information on the attenuation of PGA with distance, and it represents a relatively unstable point estimate of the average PGA that prevailed during the event at that specific distance. Campbell (1980) found the results for the weighting-by-earthquake scheme to be virtually identical to those obtained by removing the 31 records of the 1979 Imperial Valley earthquake from the analysis, thus totally discounting this very significant event.

The nine-bin weighting scheme was chosen for use in this study because it represents a reasonable balance between the two extreme cases discussed above. This approach balanced the important distance attenuation characteristics of well-recorded earthquakes with the near-source magnitude scaling characteristics of the few significant singly-recorded events. To determine the weights the range of distances used in the analysis (0 to 50 kilometers) was divided into nine intervals in which each recording was assigned a relative weighting factor of $1/n_{ij}$ where n_{ij} is the total number of acceleration recordings for the i^{th} earthquake within the j^{th} distance range. The weights were then normalized so that their sum totalled the number of recordings used in the analyses. This assured that the statistics of the analyses would represent the correct number of degrees-of-freedom. The distribution of earthquake recordings within each distance interval is presented in Table 3.

TABLE 3

DISTRIBUTION OF EARTHQUAKE RECORDINGS BY DISTANCE

Distance Range (Km)	Earthquake	No. of Recordings	Distance Range (Km)	Earthquake	No. of Recordings	
0 - 2.4	Parkfield 1966	1	14.1 - 19.9	Parkfield 1966	1	
	Imperial Valley 1979	6		Fairbanks, Alaska 1967	1	
2.5 - 4.9	Tabas, Iran 1978	1		Lytle Creek 1970	1	
	Koyna, India, 1967	1		Santa Barbara 1978	1	
	Gazli, USSR, 1976	1		Malibu 1979	1	
	Coyote Lake 1979	2		Coyote Lake 1979	2	
	Imperial Valley 1979	4		Imperial Valley 1979	2	
5.0 - 7.4	Long Beach 1933	1		San Fernando 1971	7	
	Parkfield 1966	1		20.0 - 28.2	Santa Barbara 1978	1
	Managua 1972 (m. 5.6)	1			Daly City 1957	1
	Coyote Lake 1979	1	Lytle Creek 1970		1	
	Imperial Valley 1979	5	Point Mugu 1973		1	
7.5 - 9.9	Helena, Montana	1	Bishop 1978		1	
	Daly City 1957	1	Coyote Lake 1979		2	
	Parkfield 1966	1	Long Beach 1933		2	
	Hollister 1974	1	Malibu 1979		2	
	Oroville 1975	1	Imperial Valley 1979		4	
	Bishop 1978	1	San Fernando 1971		10	
	San Fernando 1971	2	28.3 - 40.0	Bear Valley 1972	1	
	Coyote Lake 1979	2		Lima, Peru 1974	1	
	Imperial Valley 1979	2		St. Elias, Alaska 1978	1	
	Santa Barbara 1978	3		Lytle Creek 1970	2	
10.0 - 14.0	Imperial Valley 1940	1		Bishop 1978	2	
	Santa Barbara 1941	1		Imperial Valley 1979	2	
	Santa Barbara 1978	1		Oroville 1975	3	
	Hollister 1974	2		San Fernando 1971	5	
	Daly City 1957	3		40.1 - 56.6	Kern County 1952	1
	Imperial Valley 1979	5			Horrego Mountain 1968	1
		Sitka, Alaska 1972	1			
		Lima, Peru 1974	1			
		Imperial Valley 1979	1			

Regression analysis

Two types of analyses were used in conjunction with the mathematical relationship given by Equation 1 to develop ground motion models for peak acceleration. In the first, regression analysis was used to establish all coefficients in the ground motion model. In the second, regression analysis together with certain constraints were used to control the behavior of peak acceleration near the fault rupture surface and in the far field where data were lacking. Consistent with a lognormal distribution of PGA, which was later confirmed by an analysis of residuals, the regression analysis was performed on the logarithmic form of Equations 1 and 2 with peak acceleration in fractions of gravity and distance in kilometers.

Due to the nonlinear form of the distance term, the coefficients were determined from a nonlinear weighted regression analysis using the method of least squares. This analysis resulted in the following expression for the median (50th-percentile) value of PGA:

$$\text{PGA} = 0.0159 \exp(0.868M) [R + 0.0606 \exp(0.700M)]^{-1.09} \quad (3)$$

All the coefficients were found to be statistically significant at levels of confidence exceeding 99 percent, based on empirical distributions of the coefficients developed using procedures set forth by Gallant (1975). The 84th-percentile value of PGA is obtained by multiplying the median value by a factor of 1.45, which represents a standard error of 0.372 on the natural logarithm of PGA. The goodness-of-fit is represented by an r-square value of 0.81, which indicates that 81 percent of the variance in PGA is explained by the model. Plots of this relationship as a function of distance and magnitude showing the limits of applicability appear in Figures 2 and 3. It should be emphasized that predictions based on this expression represent the mean of the two peak horizontal values from a recording. If an estimate of the maximum value is required, an additional factor of 1.13 should be applied to the predicted values.

The scatter of the observations about their predicted values is shown in Figure 4 where the residuals from the regression analysis are plotted as a function of distance. For this purpose, the residuals have been weighted and normalized to have a mean of 0.0 and a variance of 1.0, as described later in this paper. A comparison of the predictions with the observed accelerations is made in Figures 5 and 6. In Figure 5 the data are grouped into magnitude intervals of 5.0-5.9, 6.0-6.9 and 7.0-7.7 and are plotted as a function of distance. Also plotted as solid lines are predicted curves for the bounding magnitude values of each interval. The dashed lines represent the 84th-percentile and 16th-percentile curves for the upper and lower bounds, respectively. Figure 6 gives a similar comparison versus magnitude for observations grouped into distance intervals of 0-9.9, 10.0-27.9 and 28-50 kilometers. The significant feature of these comparisons is the uniformity with which the predicted curves represent the observed behavior of these data.

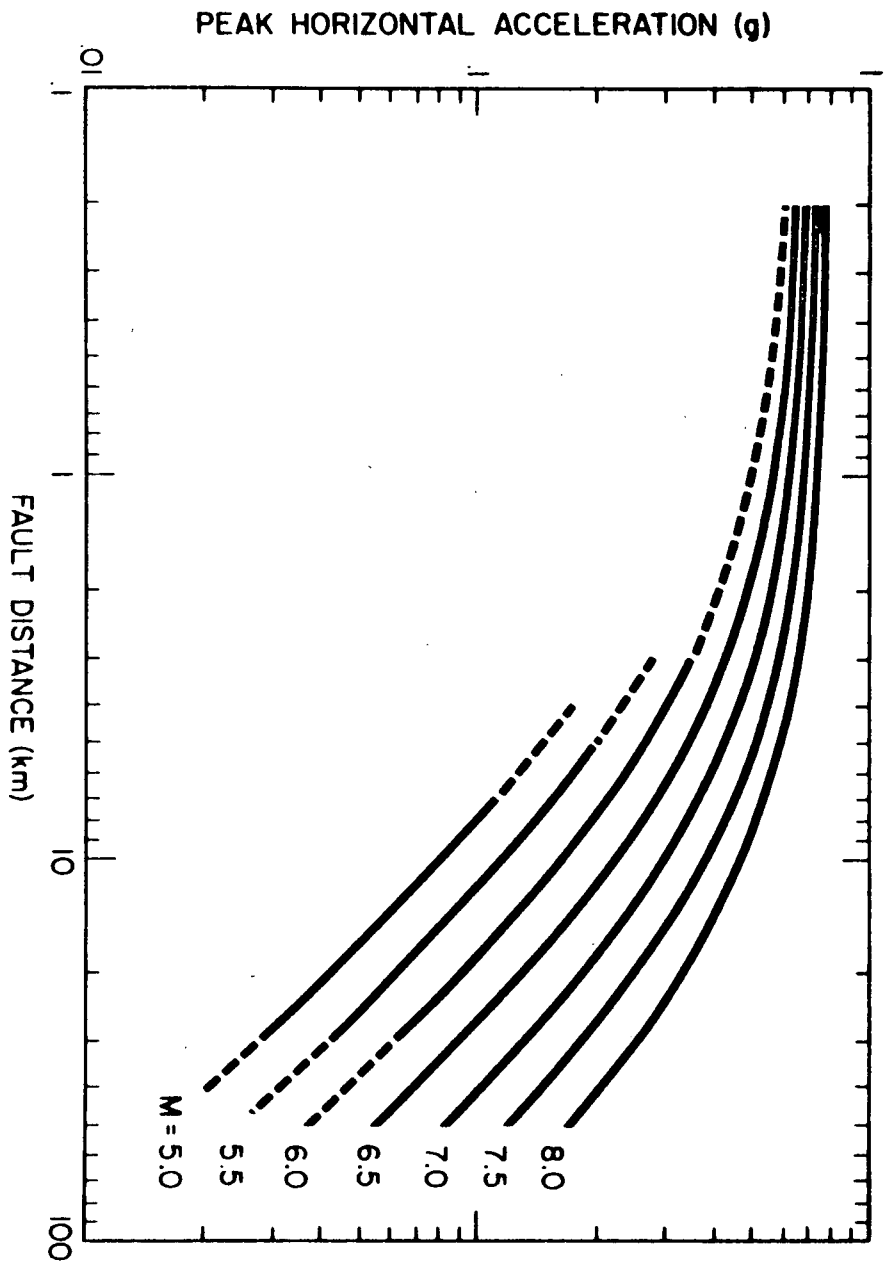


Figure 2. The unconstrained ground motion model (Eq. 3) plotted as a function of fault distance for magnitudes of 5.0 to 8.0. The dashed lines represent extrapolations of limited applicability due to either a lack of data or ambiguity as to the depth of rupture during an event.

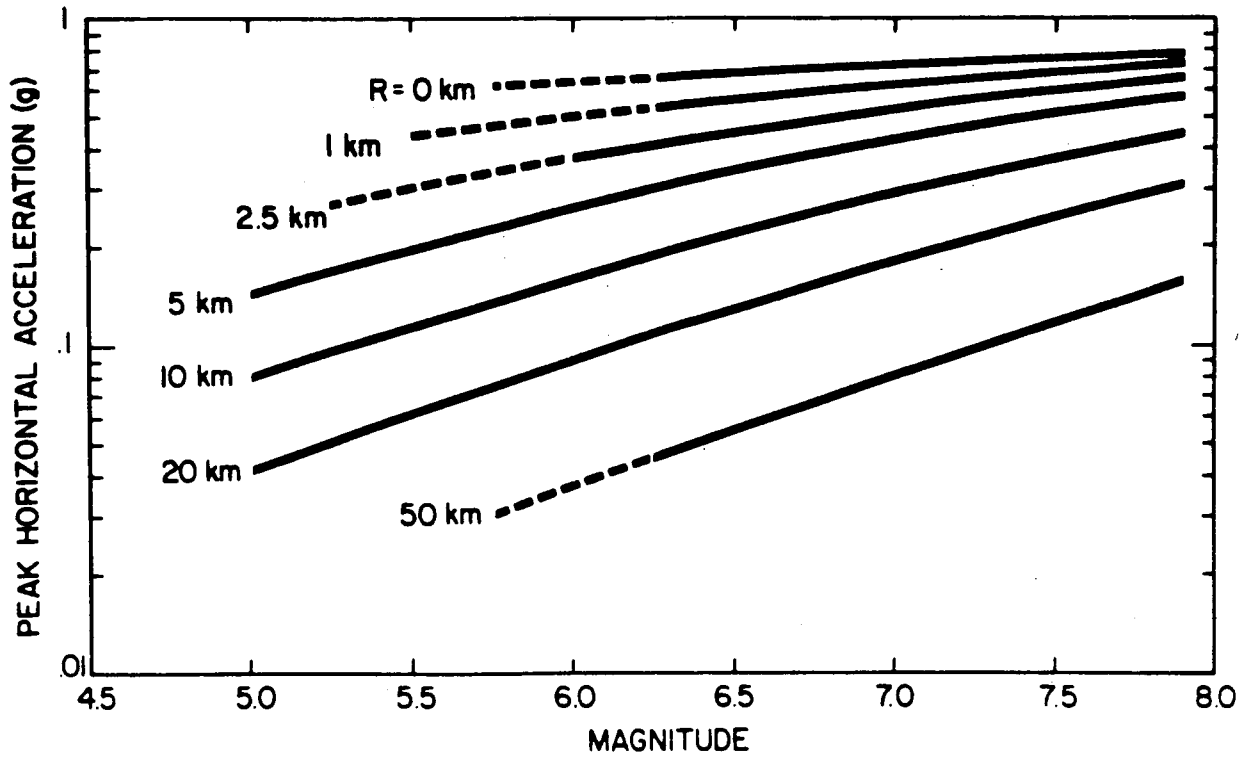


Figure 3. The unconstrained ground motion model (Eq. 3) plotted as a function of magnitude for fault distances of 0 to 50 kilometers. The dashed lines represent extrapolations of limited applicability due to either a lack of data or ambiguity as to the depth of rupture during an event.

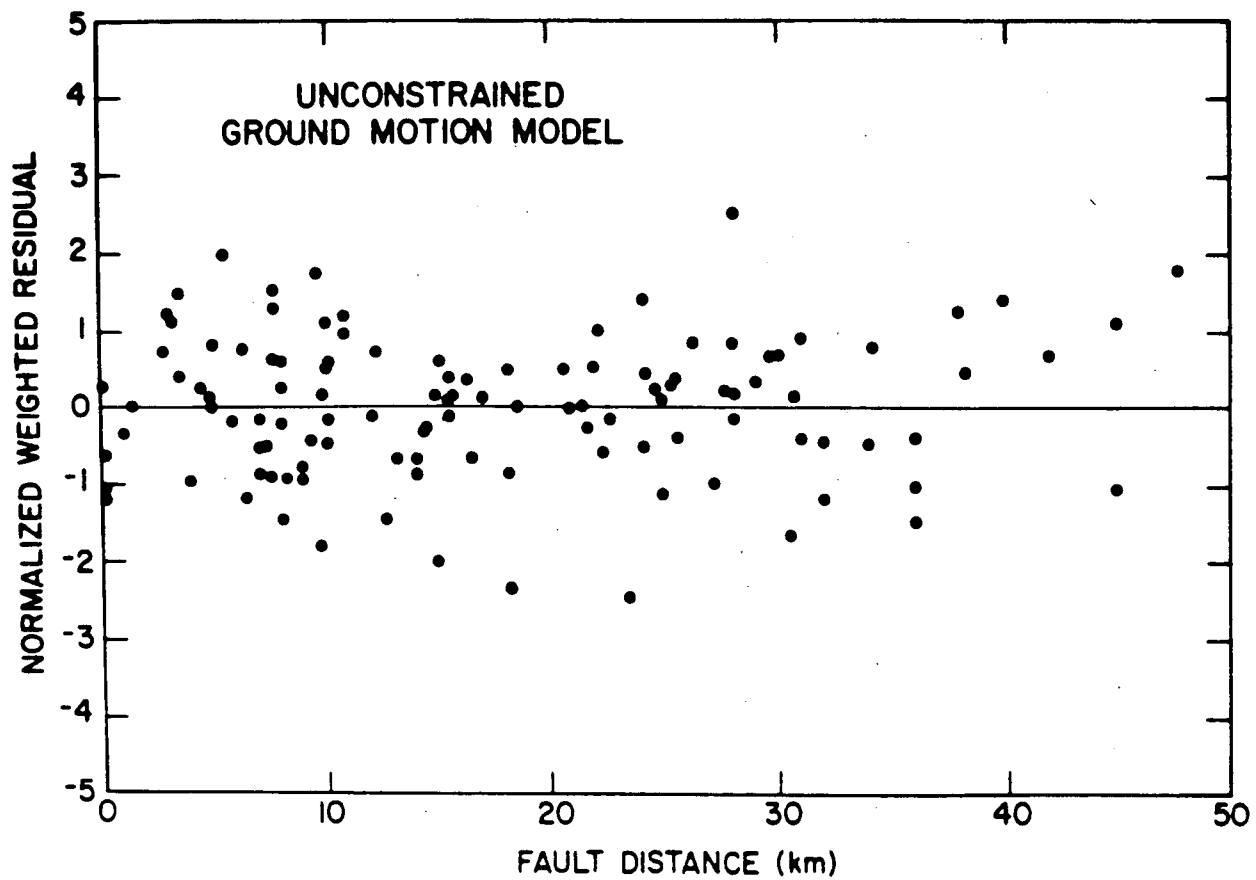


Figure 4. A plot of residuals as a function of fault distance for the unconstrained regression analysis (Eq. 3). The residuals have been weighted and normalized to have a mean of zero and a variance of unity.

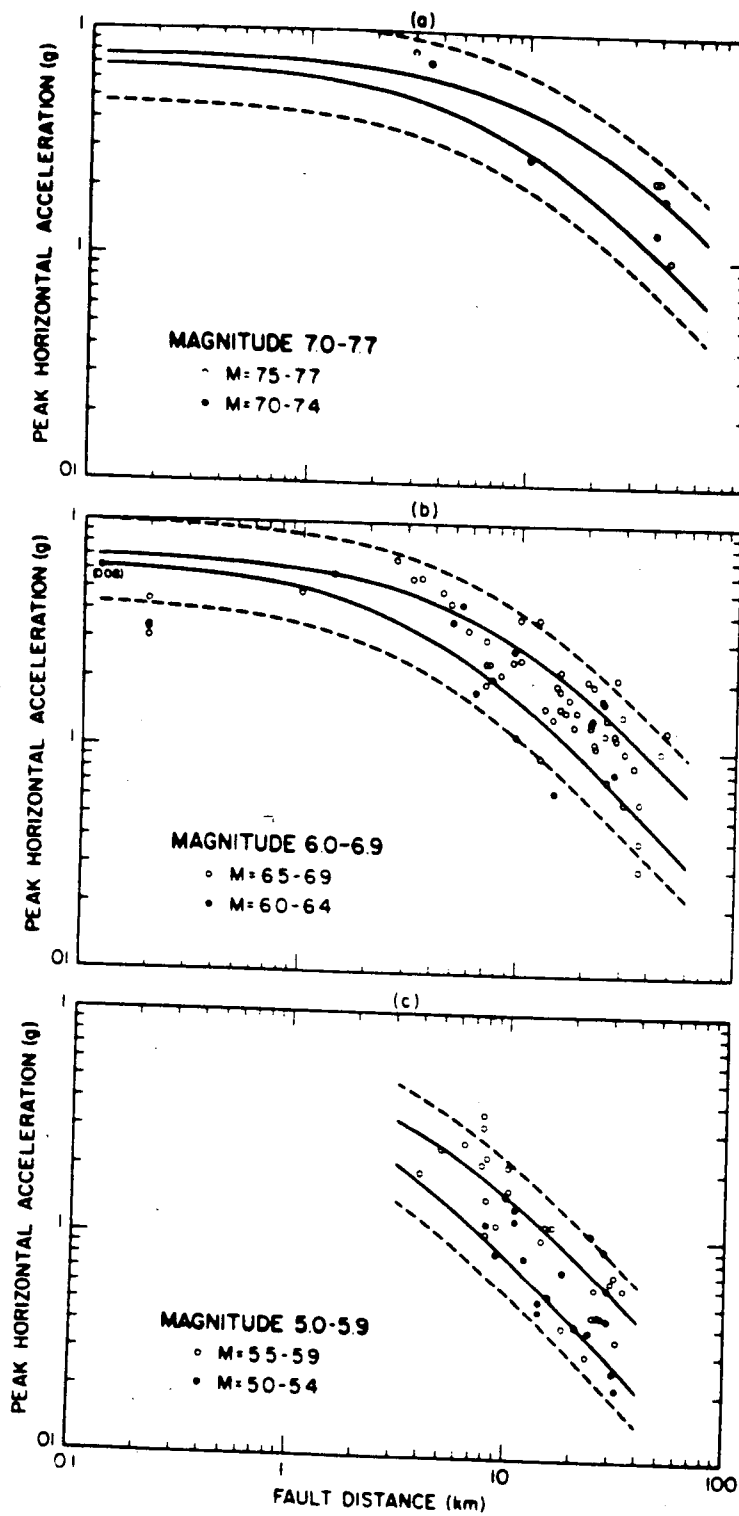


Figure 5. A comparison of the observed values of peak horizontal acceleration with the predictions of Eq. 3 for magnitude intervals of a) M 7.0-7.7, b) M 6.0-6.9 and c) M 5.0-5.9. The solid lines represent the median predictions for the bounding values of magnitude for each interval, and the dashed lines represent the 84-percentile and 16-percentile predictions for the upper and lower bound magnitudes, respectively.

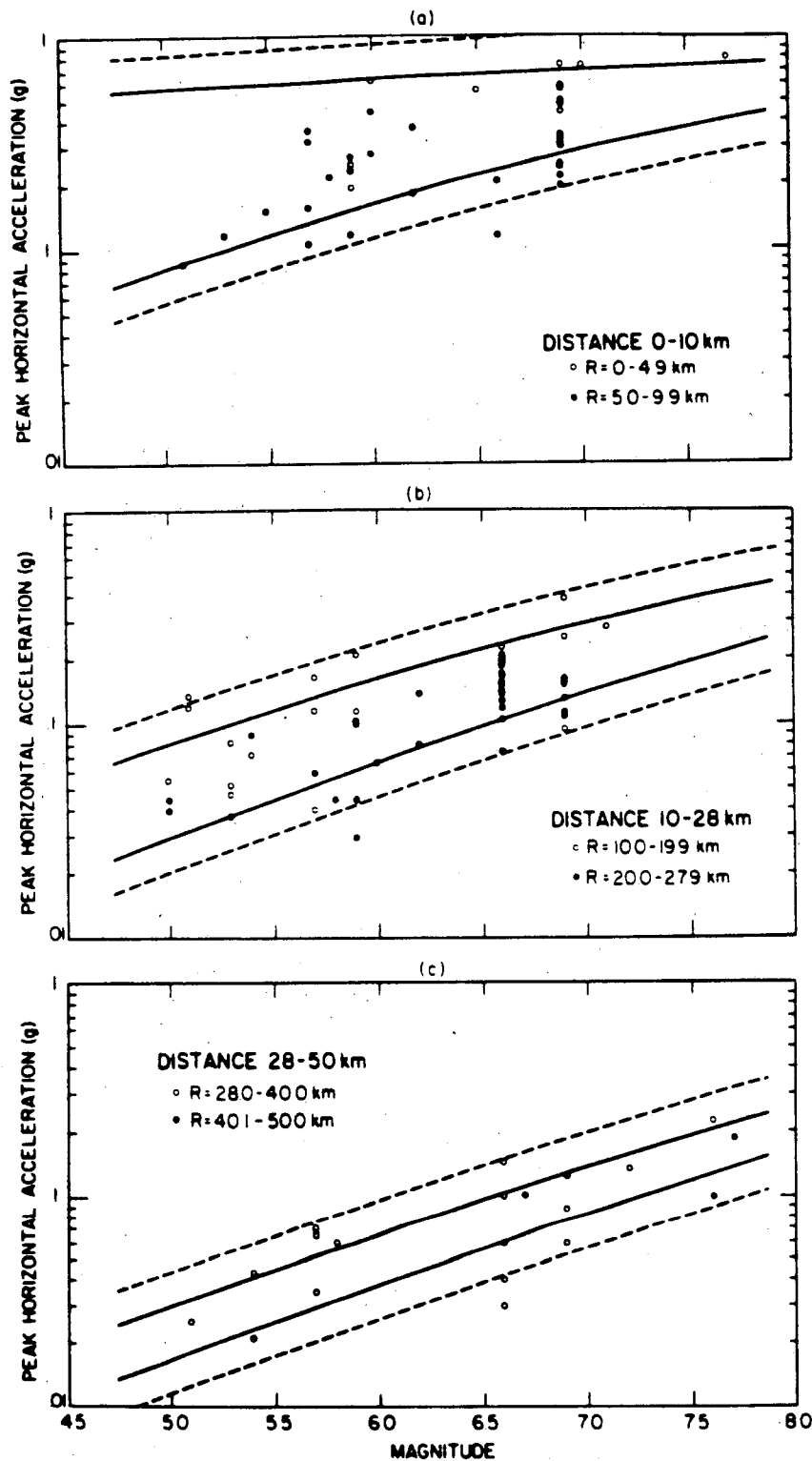


Figure 6. A comparison of the observed values of peak horizontal acceleration with the predictions of Eq. 3 for distance intervals of a) 0-10 km, b) 10-28 km and c) 28-50 km. The solid lines represent the median predictions for the bounding values of distance for each interval, and the dashed lines represent the 84-percentile and 16-percentile predictions for the upper and lower bound distances, respectively.

Near-Field and Far-Field Constraints

Because this study was not directly concerned with predicting far-field ground motions, peak accelerations recorded farther away than 30 or 50 kilometers from the source were not included in the analysis. In order for the predictions of PGA to be consistent with far-field data and give more realistic values at larger distances, the far-field attenuation rate \underline{d} of Equation 1 was constrained to a value of 1.75 in a second analysis. This value was selected from a survey of published attenuation relationships as being representative of the far-field attenuation of PGA.

A second, near-field constraint involved the prediction of PGA at distances closer than three to five kilometers from the fault, where strong-motion data are extremely limited. Many seismologists and geophysicists currently believe that at or very near the rupture surface peak accelerations become essentially independent of earthquake magnitude (Ambraseys, 1969, 1973, 1978; Brune, 1970; Dietrich, 1973; Trifunac, 1973; Jennings and Guzman, 1975; Hanks and Johnson, 1976; Bolt, 1978; Midorikawa and Kabayashi, 1978; Seekins and Hanks, 1978; Del Mar Technical Associates, 1979; Hanks, 1979; Aki and Richards, 1980; Hadley and Helmberger, 1980; McGarr, 1980; McGarr et. al., 1981). In particular, the interpretation of the physics of the rupture process by Del Mar Technical Associates (1979) indicates that PGA should be controlled by dynamic stress-drop, a quantity related to the strength of rock on the fault rupture surface, not by the dimensions of the rupture or the amount of fault displacement. Based on this argument, a further constraint was included in the second analysis that required a constant peak acceleration, independent of magnitude, at the fault rupture surface. This condition required that the parameter c_2 in Equation 2 be given by the expression

$$c_2 = \frac{b}{d} \quad (4)$$

The second regression analysis resulted in the following expression for the median (50th-percentile) value of peak acceleration:

$$PGA = 0.0185 \exp(1.28M) [R + 0.147 \exp(0.732M)]^{-1.75} \quad (5)$$

Application of the empirical procedure of Gallant (1975) determined the unconstrained coefficients of this expression to be statistically significant at levels of confidence exceeding 99 percent. The 84th-percentile value of PGA is obtained by multiplying the median value by a factor of 1.47, which represents a standard error of 0.384 on the natural logarithm of PGA. The goodness-of-fit is represented by an r-square value of 0.79. The scatter in the data about their predicted values is given in Figure 7. This may be compared to a similar plot for the unconstrained model, Figure 4.

A comparison of the ground motion model given by Equation 5 and that given by the unconstrained analysis is made in Figure 8. Differences between these models are found to be relatively small compared to the standard error

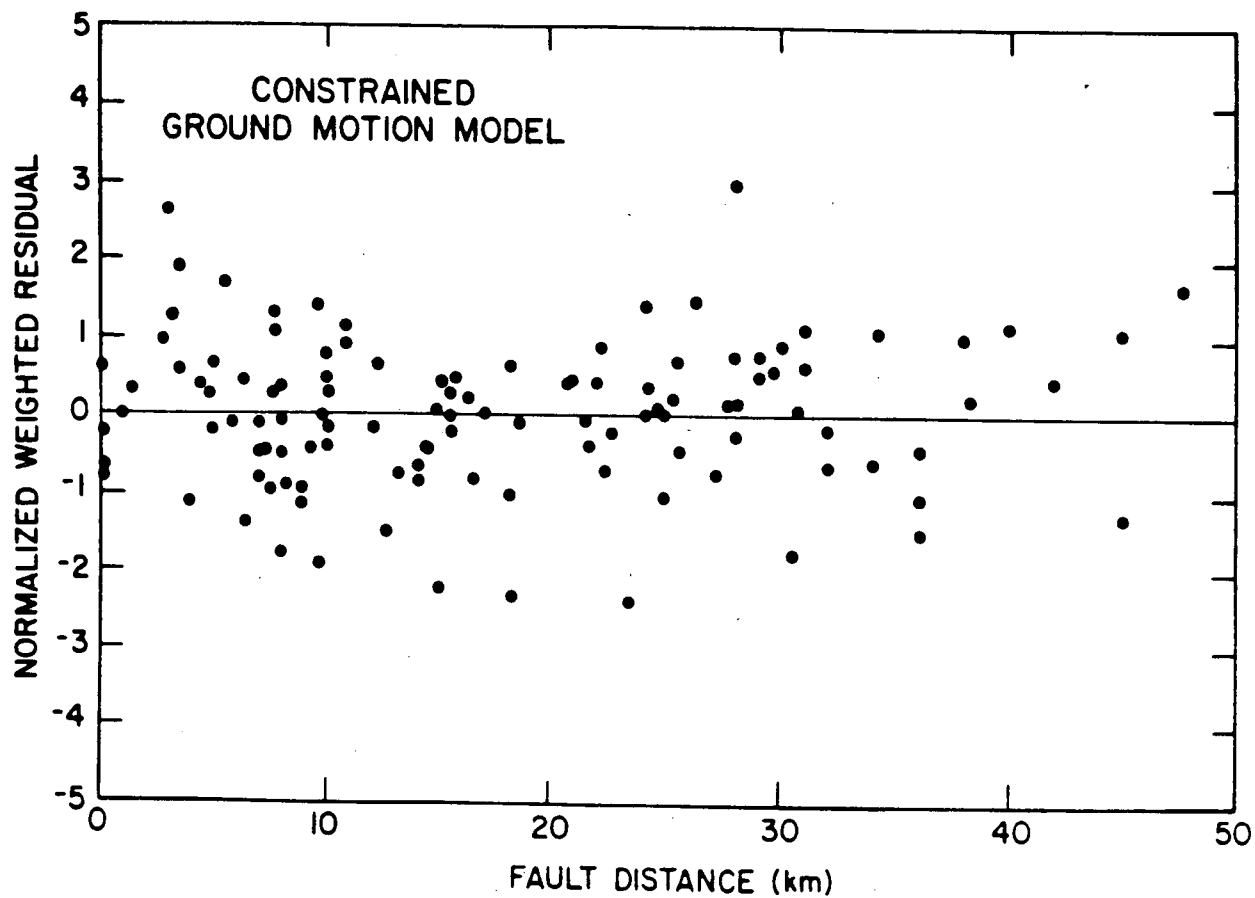


Figure 7. A plot of residuals as a function of fault distance for the constrained regression analysis (Eq. 5). The residuals have been weighted and normalized to have a mean of zero and a variance of unity.

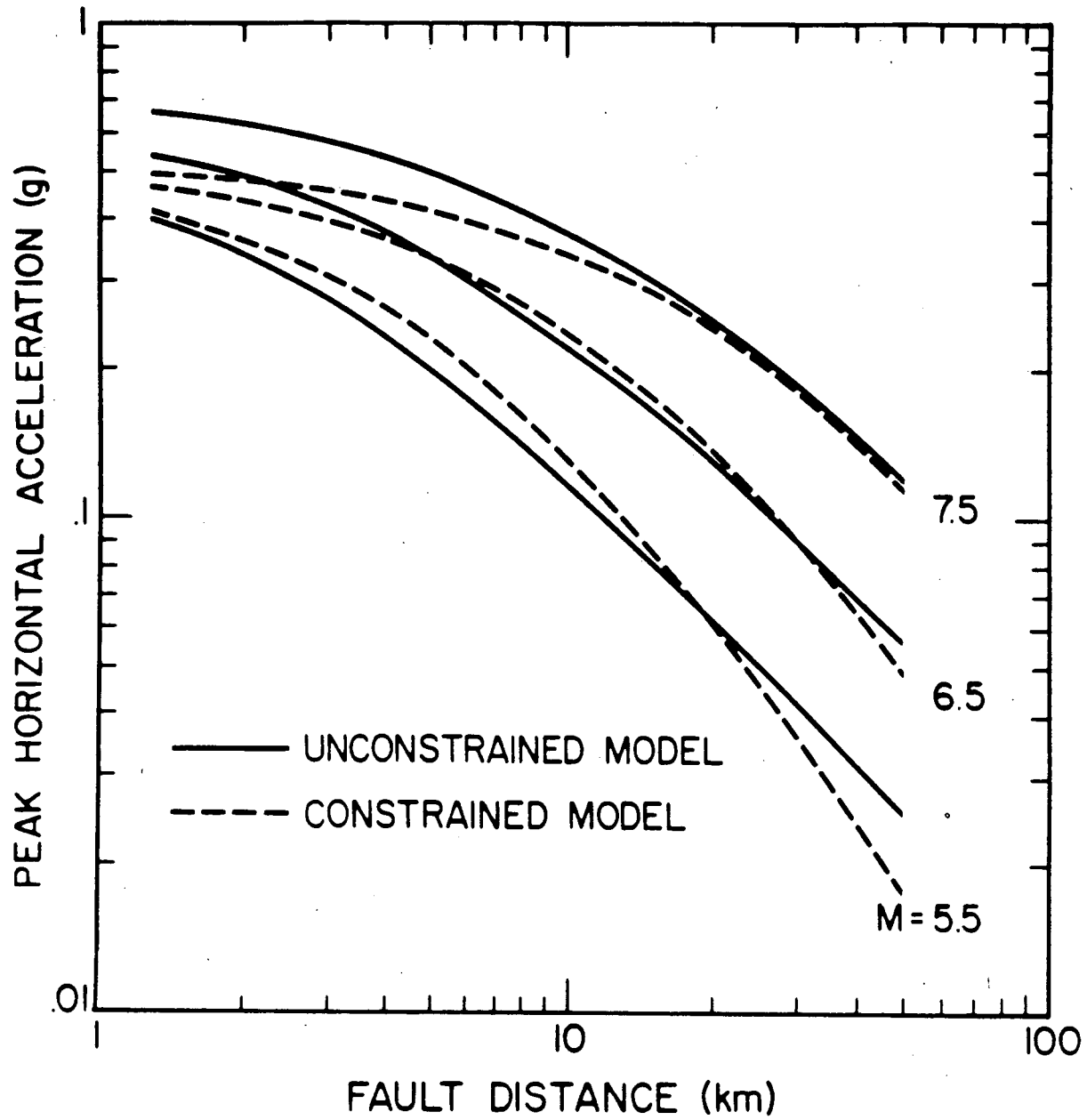


Figure 8. A comparison of the unconstrained and constrained ground motion models for magnitudes of 5.5, 6.5 and 7.5.

associated with their predictions. This reflects a large reduction in magnitude scaling in the near field that is statistically supported by the data.

GROUND MOTION CHARACTERISTICS

Residuals resulting from the regression analyses described above were analyzed to study the effect of various parameters on the amplitude, attenuation and magnitude scaling of PGA. For this purpose, a residual was simply defined as the difference between the observed and predicted value of the natural logarithm of PGA for the specified value of magnitude and distance.

Before analysis, each residual was transformed into a normalized weighted residual (NWR). The weighting was required to make each residual consistent with that used in the weighted least-squares analyses employed in the regression. Weighted residuals were then normalized to have a mean of 0.0 and a variance of 1.0 for the sake of consistency and ease of computation and plotting. Letting n equal the number of total observations used in the regression, the normalized weighted residual for the i^{th} observation was computed from the equation

$$NWR_i = \frac{[\sqrt{w_i} (\ln PGA_i - \overline{\ln PGA_i})]}{\sigma} - MWR \quad (6)$$

where

$$MWR = \frac{1}{n} \sum_{i=1}^n \sqrt{w_i} (\ln PGA_i - \overline{\ln PGA_i})$$

$$\sum_{i=1}^n w_i = n$$

In these expressions w_i is the weight used in the regression analysis, $\ln PGA_i$ is the observed value, $\overline{\ln PGA_i}$ is the predicted value, σ is the standard error of the regression, and MWR is the mean weighted residual.

Three types of analyses were used to test the effect of various parameters on PGA. In the first analysis, the mean normalized weighted residual (MNWR) for each subset, selected on the basis of the parameter under study, was compared to a value of 0.0 appropriate for the entire population, where MNWR is given by the expression

$$MNWR = \frac{1}{n_j} \sum_{i=1}^{n_j} NWR_i \quad (7)$$

and n_j represents the number of observations in subset j . In the second analysis, the variance of each subset was compared to the population variance of 1.0. The

third analysis consisted of visual inspection of the normalized weighted residuals plotted as a function of distance, magnitude and predicted value together with an accompanying correlation analysis to determine possible trends between the residuals and these three variables. Standard hypothesis testing techniques were used to test the significance of observed variations (e.g., Bowker and Lieberman, 1972).

For the purposes of this study, differences in the residuals were neglected if they were not found to be significant at a level of confidence of 90 percent or greater. Those parameter subsets found to be significantly different from the population are discussed below.

Distribution of Residuals

In order to test for potential biases in the predictions given by Equations 3 and 5 regarding magnitude, distance or predicted acceleration, plots of the normalized weighted residuals with respect to these three parameters were carefully inspected. Two such examples of these plots appear as Figures 4 and 7. If there were systematic trends in the data that were not accounted for by our statistical analysis, such trends would be evident from these plots. However, the residuals were found to be uniformly distributed with respect to magnitude, distance and the predicted accelerations. A correlation analysis confirmed that the residuals were uncorrelated with respect to these variables at a greater than 99-percent level of confidence.

Many of the statistical tests used in the analysis of residuals required the assumption that the residuals be distributed normally. Since the regression analysis was performed on the logarithm of peak acceleration, this would require PGA to be lognormally distributed. The observed distribution of the normalized weighted residuals of the regression leading to Equation 3 is given in the insert of Figure 9. Visual inspection of this histogram would appear to confirm the assumption of normalcy. A more statistical validation may be obtained from the normal probability plot presented in the same figure where the normal score, an estimate of the cumulative distribution function of the residuals, is plotted against the normalized weighted residuals. The linear trend of this plot again suggests that the residuals are normally distributed. A Kolmogorov-Smirnov test confirmed that the assumed normal distribution fell within the 90-percent confidence limits of the actual distribution, a criterion commonly used in engineering applications; thus, PGA could be accepted as being lognormally distributed. Similar results were obtained for the constrained model (Equation 5).

Site Geology Effects

As has been noted by other investigators (e.g., Boore et al., 1980; Crouse, 1978), the potential effects of site geology were subject to possible contamination by structural effects. For instance, most of the recordings in the data base used for analysis were obtained in buildings sited on soil. Furthermore, the larger the building, the more likely the instrument was located in a basement. Thus, the effects of site geology, building size and instrument location were found to be extensively interrelated. We attempted to segregate the effects of site geology

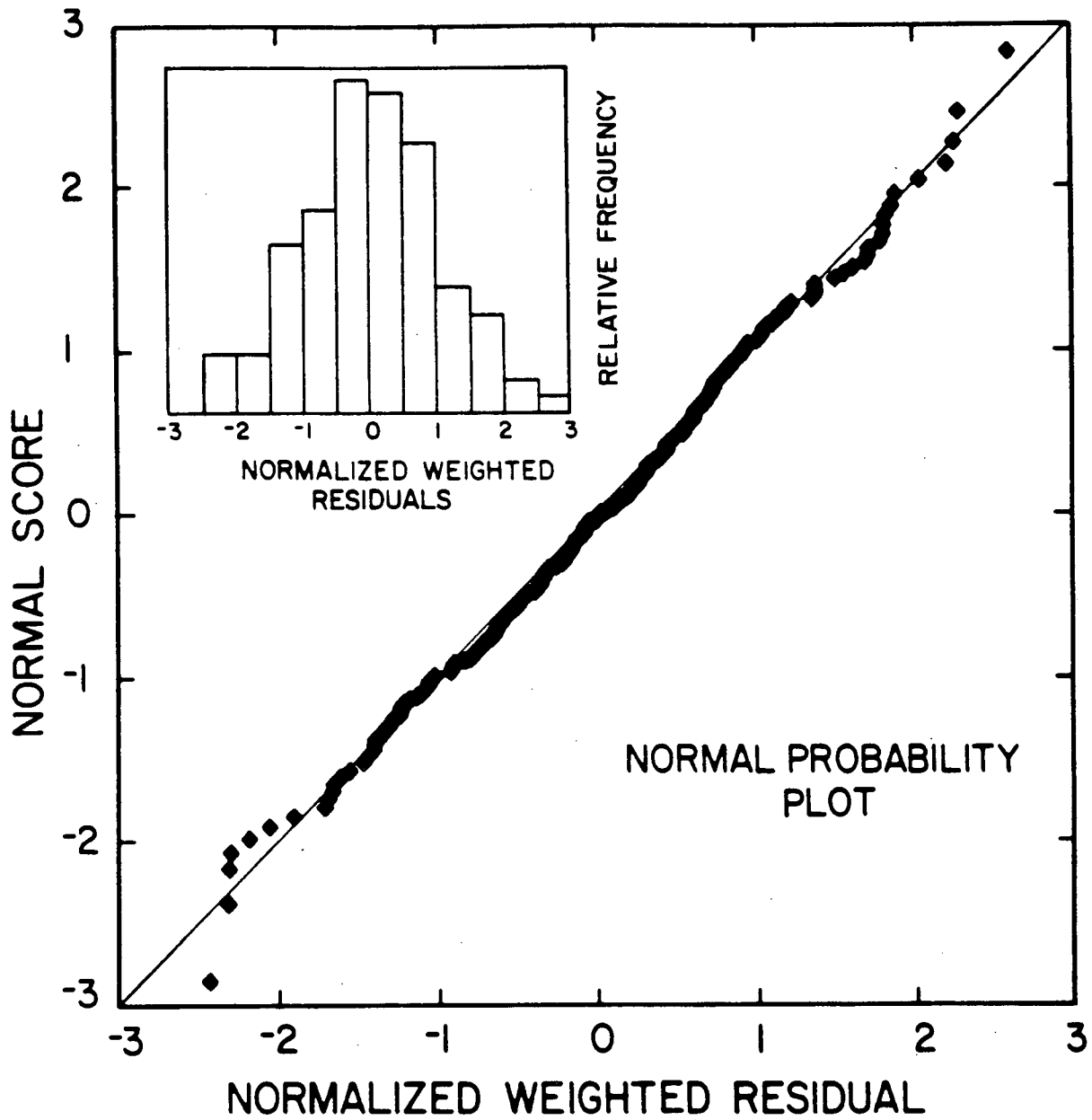


Figure 9. A normal probability plot comparing the observed distribution of residuals for the unconstrained ground motion model with that based on a normal distribution. Residuals have been weighted and normalized to have a mean of zero and a variance of unity.

from these other effects by selecting data recorded at ground level in the free field or in small structures (one- and two-story buildings consistent with Boore et al., 1980) which represented 161 components of PGA.

Sites were initially classified into the six groups described in Table 2 based on geotechnical and geological descriptions available in the literature or from geology maps. Those sites originally classified as rock sites (Types C and D) or suspected of being shallow soil deposits were further subjected to a field visit by an engineering geologist who obtained an accurate description of the site geology, topography and instrument location for each of these sites. This investigation revealed that about half of the sites originally determined to be rock either by us or other investigators were actually found to be overlain by shallow soil or fill.

To study the significance of these findings, ground motion models similar to Equations 3 and 5 were first developed by combining data from all geologic classifications (Types A through F) to test the potential bias of the shallow soil sites. For this purpose, the 16 shallow soil sites (32 components) were separated into those having soil depths of five meters or less and those whose soil depths were between five and ten meters. Both groups were found to have a mean weighted residual that was significantly higher at a 90-percent level of confidence than the average value of 0.0 for all geology types. Their combined effect represented on the average an 84-percent higher PGA as compared to predictions based on the other geologic classifications. This factor was found to decrease to a value of 63 percent when a reverse-fault variable was included. Due to the significance of this bias and the uniqueness of these site conditions, shallow soil deposits were not included for all subsequent analyses.

Although predictions of PGA were found to be essentially unaffected by the presence of shallow soil deposits in the data base due to the small number of recordings, the real bias in these data came from their influence on conclusions regarding the effect of site conditions on recorded ground motion. In the past investigators have included sites having as much as five to ten meters of soil overlying rock as rock sites in their analyses of site type. To test the significance of this bias, we divided our sites into soil and rock and developed two ground motion models: one including shallow soil deposits as rock and one excluding them altogether. When they were included as rock, we found PGA recorded on rock sites to be on the average 26-percent higher than those recorded on soil sites, significant at a 90-percent level of confidence. When shallow soil sites were excluded, differences in accelerations recorded on soil and rock were not found to be statistically significant, consistent with the findings of Boore et al. (1980).

The Punaluu, Hawaii site founded on beach sand was the only strong motion station recording a $M \geq 5.0$ earthquake that was classified as a soft soil deposit. The mean horizontal PGA recorded at this site was found to be about 30-percent lower than that predicted by Equation 3. Since soft soil deposits represent a unique site condition not encountered in most siting studies, this site was not included in all subsequent regression analyses.

Once shallow soil and soft soil deposits were removed, new ground motion models were developed to study the effect of the other site types. In studying these results, we found the variation in the mean residual for each geology classification to be insignificant, which leads to the conclusion that once shallow and soft soil sites are removed the effect of geology is negligible compared to other factors that contribute to the scatter in PGA. Therefore, it was decided to include geologic classifications A through D and exclude classifications E and F in the development of the ground motion models given by Equations 3 and 5. The proportion of data in each of the classifications used in the final analysis is given in Table 4.

We emphasize that these conclusions are valid only for peak accelerations in the near-source region of $M \geq 5.0$ earthquakes and cannot be extended without further study either to other ground motion parameters such as peak velocity, displacement, or spectral ordinates or to further distances or smaller magnitudes.

Effect of Fault Type

Of the 27 earthquakes used in this study, faulting mechanisms of 14 are strike-slip, nine are characterized by reverse or thrust mechanisms, two are normal and the remaining two are a combination of strike-slip and dip-slip faulting. The inference is based on geological field reports, seismological source studies and tectonic environments.

The distribution of the acceleration data according to earthquake fault type is given in Table 4. As seen in this table, while all types of faulting are represented in the data base, the majority of the data are strike-slip (about 61 percent), similar to faults of the San Andreas system. As with geology, the effects of fault type were also found to be influenced by the presence of data recorded within large structures. Therefore, for uniformity only small structures and free-field stations were used for the analysis of fault type.

The analysis of residuals demonstrated that accelerations from reverse faults are systematically higher than those from other fault types, predominantly strike-slip, significant at the 90-percent level. The magnitude of the bias was found to reflect the presence of non-North American data. For instance, accelerations from reverse faults were found to be on the average 28-percent higher than those from other fault types based on the worldwide data set. When non-North American data were removed, this factor reduced to 17 percent. These differences are indicative of the strong bias introduced by the 1974 Lima, the 1976 Gazli, and the 1978 Tabas earthquakes which all had reverse source mechanisms.

Building Effects

In order to isolate the effects of building size and embedment from geologic effects, the data base was divided into four subgroups, all situated on soil (Types A and B), represented by embedded and ground-level recordings in small (one- or two-story) buildings or free-field stations and in large (three- to twenty-story) buildings.

TABLE 4
 DISTRIBUTION OF RECORDINGS WITH RESPECT
 TO GEOLOGY AND FAULT TYPE

Parameter	Number of Recordings	Percent of Total
Geological Classification		
Recent Alluvium	71	61
Pleistocene Deposits	22	19
Soft Rock	14	12
Hard Rock	9	8
Fault Type Classification		
Strike-Slip	69	59
Reverse	40	35
Normal	5	4
Oblique	2	2

The effects of both embedment and building size were studied by regression analysis of the above selected data. Due to limitations in these data, valid comparisons could only be made between small building/free-field recordings (58 recordings) at ground level and recordings obtained in the lowest basement of large buildings (20 recordings). This comparison indicated that PGA recorded in the basement of large buildings was on the average 24-percent lower than those recorded at ground level, significant at the 90-percent level of confidence. This value is somewhat less than the average reduction of 34 percent reported in a case study by Darragh and Campbell (1981) for a similar comparison of peak accelerations recorded by nearby ground-level and embedded instruments.

Effect of Steep Topography

A site investigation by an engineering geologist identified seven stations (representing 13 components of PGA) in the data base considered to be located within an area of steep topographic relief, defined as the top or side of a steep ridge, hill or slope. In addition, four stations classified as shallow soil deposits and the Pacoima Dam station were also found to be located in areas of steep topographic relief.

A statistical analysis of the seven stations used in the regression revealed that their mean residual was significantly higher than that for the entire data set, this bias being significant at the 90-percent level. Due to the small number of stations, however, the magnitude of this bias is probably not reliable and is not reported here. Similar results were obtained for the 11 topographically affected stations when shallow soil sites were included in the regression analysis. When the topographically affected stations were excluded from the analysis, predictions of PGA were found to be essentially unaffected, a result of the relatively small number of such records.

Although this bias could be the result of factors other than topography, such an explanation for the above results is not considered reasonable. Of the seven stations used in the analyses, three are located on abutments of dams, two are located in small buildings, and two are located in large buildings. Of the five earthquakes represented, two of them (7 components) have reverse or thrust mechanisms and three of them (6 components) have strike-slip mechanisms. While all of the stations are located on rock, four are situated on hard rock and three on soft rock.

The Pacoima Dam recording from the 1971 San Fernando earthquake has been the subject of much investigation in the past. The strong-motion station is located on a narrow rocky ridge near the south abutment of a 113-meter-high thin concrete arch dam. Boore (1973) used a simple topographic model together with finite difference techniques to estimate the effect of the instrument location on the recorded accelerations. He found that the peak acceleration from the S16⁰E component of the accelerogram may have been amplified by as much as 50 percent due to the effect of topography.

Mickey et al. (1973) empirically studied the combined effects of topography, response of the dam, and local geological conditions on the Pacoima Dam recording. They simultaneously recorded eight aftershocks (M_L 2.7-3.7) at three

stations on the dam crest, at the strong-motion station and at a free-field site located on rock on the valley floor downstream from the dam. Their results indicated an average amplification of 75 percent in the peak motion recorded at the strong-motion station as compared to the free-field site for the $S16^{\circ}E$ component and an average amplification of 190 percent for the $S74^{\circ}W$ component. The large amplification for the $S74^{\circ}W$ component was thought to be due in part to the response of the dam, as interpreted from the recordings obtained on the crest of the dam and studies by Reimer et al. (1973).

If we apply the average amplification factor obtained by Mickey et al. (1973) to the peak horizontal acceleration of 0.43 g predicted by Equation 3 for the Pacoima Dam strong-motion site ($M_S = 6.6$, $R = 3.2$ km), we obtain a value of 1.0 g. If we further take into account a 17 to 28 percent increase in PGA due to the reverse mechanism of the San Fernando event, we obtain a PGA of 1.17 g to 1.28 g, values consistent with the mean peak horizontal acceleration of 1.25 g recorded during this event. Therefore, we find our predictions quite consistent with the Pacoima Dam recording when account is taken for the unusual site conditions at the station.

More evidence in support of an anomalously high PGA for the Pacoima Dam recording is the Koyna Dam recording obtained during the $M_S 6.5$ Koyna, India, earthquake of 1967, a strike-slip event of almost the same magnitude as the San Fernando earthquake. This station, located near the base of the dam and about three kilometers from the rupture surface, recorded a mean peak horizontal acceleration of 0.56 g, less than half of that obtained at the Pacoima Dam site.

SENSITIVITY STUDIES

A study was conducted to determine the sensitivity of the predictive ground motion models (Equations 3 and 5) with respect to the data base, selection criteria and various assumptions incorporated in the analyses. Studies were concentrated in six main areas: (1) the effect of the functional form of the scaling relationships, (2) the effect of the far-field attenuation rate, (3) the effect of the data selection criteria, (4) the effect of using fault distance, (5) the effect of large structures, and (6) the effect of the definition of PGA.

Functional Form

In addition to the unconstrained and constrained models defined by Equations 3 and 5, respectively, four additional scaling models were proposed and developed for this study to check the sensitivity of the results to the selected form of the ground motion models.

Four of the six models involved the choice of the parameter $C(M)$ in Equations 1 and 2. In the first, the unconstrained model, the parameters c_1 and c_2 were allowed to be statistically fit by the regression analysis. In the second, the constrained model, c_2 was determined by Equation 4. In the third model, $C(M)$ was constrained to be a constant independent of magnitude (i.e., $c_2 = 0$). In the fourth model, $C(M)$ was set equal to zero and the remaining constants fit by the

regression. In all but the constrained model, the far-field attenuation rate was determined from the regression analyses. Near-field properties of the four models involving the choice of $C(M)$ are described in Table 5.

A fifth model, with properties similar to a relationship proposed by Donovan and Bornstein (1978), was a log-linear relationship of the form

$$\ln \text{PGA} = A + BM + \ln R \left[D + EM + F (\ln R) \right] \quad (8)$$

This model was chosen for comparison with Equation 1 because (1) it provided a totally different functional form and, thus, an independent approach, (2) it could incorporate magnitude and distance scaling as a function of distance, and (3) its coefficients could be determined using linear regression analyses.

A sixth model was based on the functional form proposed by Joyner and Boore (1981),

$$\text{PGA} = a \exp(bM) R^{h-d} \exp(eR^f) \quad (9)$$

$$R^f = \sqrt{R^2 + C(M)^2}$$

To accommodate magnitude and distance scaling as a function of distance, $C(M)$, as defined by Equation 2, was used in place of Joyner and Boore's constant coefficient h in the expression for R^f . Due to a lack of far-field data in our data base, an initial analysis indicated that the coefficient e should be set equal to zero. The remaining coefficients in the expression were then determined from weighted nonlinear regression analysis as was applied in the development of the unconstrained model.

Median predictions at eight kilometers for magnitudes 6.5, 7.0 and 7.5 for these various models are presented in Table 6. Also included in this table are the ratios of the median plus one-standard-deviation estimates to the median value and the r -square values (goodness of fit) of the regression.

The results of an F -test on the mean square errors from each of these models as compared to the unconstrained model indicated at a 90-percent confidence level that only the $C(M) = \text{zero}$ model had a significantly larger variance. However, the inadequacy of both this and the $C(M) = \text{constant}$ model in characterizing the near-source behavior of PGA is discussed in some detail in the Discussion. The log-linear model was found to give results consistent with the unconstrained model. However, since its mathematical form provided little insight into the behavior of near-source accelerations as compared to Equation 1, the log-linear model was not explored further in this study. At eight kilometers the Joyner and Boore model was found to give predictions about six-percent higher than the unconstrained model due to a more abrupt transition from near-field to far-field attenuation properties.

The sensitivity to the simultaneous application of both near-field and far-field constraints in the development of the constrained model was tested by applying each constraint separately. In the first test, total magnitude saturation was required at the fault rupture surface by imposing the constraint given by Equation 4. In the second test, the far-field attenuation rate d was constrained

TABLE 5

NEAR-FIELD PROPERTIES OF THE FOUR GROUND-MOTION MODELS
CONTAINING THE FUNCTION C(M)

Model	C(M)	Remarks
Unconstrained	$c_1 \exp(c_2 M)$	Near-field scaling of PGA is statistically determined.
Constrained	$c_1 \exp(bM/d)$	Near-field scaling is constrained to make PGA independent of magnitude at the fault rupture surface.
C(M) = constant	c_1	Near-field scaling of PGA with distance is statistically determined; near-field scaling with magnitude is constrained to be equal to far-field scaling, i.e., $\exp(bM)$.
C(M) = zero	0	Near-field scaling of PGA with both distance and magnitude is constrained to be equal to far-field scaling, i.e., $\exp(bM)R^{-d}$.

TABLE 6
SENSITIVITY RESULTS FOR VARIATIONS IN FUNCTIONAL FORM

Model	Peak Acceleration at 8 km(g)			$\frac{\text{Median} + 1\sigma}{\text{Median}}$	r^2
	6.5	7.0	7.5		
Unconstrained	0.26	0.33	0.42	1.45	0.81
Constrained	0.27	0.33	0.37	1.47	0.79
C(M) = Constant	0.25	0.35	0.49	1.47	0.79
C(M) = 0	0.20	0.27	0.36	1.58	0.70
Log-Linear	0.25	0.32	0.41	1.45	0.82
Joyner and Boore	0.26	0.35	0.46	1.45	0.81

to 1.75. By applying each constraint separately, the predictions at a distance of eight kilometers were found to agree closely with those of the unconstrained model, varying by six percent or less for magnitudes of 6.5 to 7.5.

Far-Field Attenuation Rate

The far-field attenuation rate \underline{d} was constrained to a value of 1.75 in the development of the constrained model consistent with other investigators' far-field studies. The sensitivity of the predictions of the constrained model to this assumption in the near field was studied by varying the assumed value of \underline{d} . In the first analysis we allowed the parameter to be fit by the regression, which selected a significantly smaller value of 1.07. This unrealistic value of \underline{d} reflects the limitation of near-source data in defining a far-field attenuation rate. Two additional analyses constrained this parameter to values of 1.5 and 2.0, respectively. The range of values selected represent a reasonable variation of this parameter, as determined from a literature survey of available attenuation models.

The results of the analyses are presented in Table 7. Variations in predictions of PGA at eight kilometers for magnitudes of 6.5 to 7.5, as compared to the constrained model, are less than eight percent, demonstrating relative insensitivity to this parameter. An F-test on the mean square errors also confirmed that there was no significant difference among these models at the 90-percent confidence level.

Data Selection Criteria

Peak acceleration data were excluded from analysis for a variety of reasons. The impact of excluding these data on the predictions of PGA for moderate to large magnitude earthquakes is assessed in this section.

There are essentially two classes of data of $M \geq 5.0$ that were excluded from analysis. The first class (hereafter referred to as Class I) represents data that were originally included as part of the general near-source data base, but were subsequently excluded from the selected data base used in the regression analyses. These data met all the general criteria outlined in the beginning of the section describing the near-source data base but did not pass the subsequent criteria used to select data for analysis. The second class of data (hereafter referred to as Class II) were originally excluded as part of the near-source data base, not passing the general criteria.

Class I Data: A summary of Class I data together with a brief description of the reasons for their exclusion is summarized in Table 8. They are represented by relatively modern events, being recorded within the last 13 years.

The impact of excluding shallow soil sites was assessed by an analysis limited to data from small structures and free-field sites consistent with our analyses on geologic effects. Regressions based on the unconstrained model were compared to a similar regression that included the 16 recordings from shallow soil sites. Predictions of PGA at a distance of eight kilometers for magnitudes of 6.5 to 7.5

TABLE 7

SENSITIVITY RESULTS FOR VARIATIONS
IN FAR-FIELD ATTENUATION RATE FOR
THE CONSTRAINED MODEL

Attenuation Rate (d)	Peak Acceleration at 8 km(g)			Median + 1σ Median	r ²
	6.5	7.0	7.5		
1.07	0.26	0.33	0.40	1.46	0.81
1.50	0.27	0.33	0.38	1.47	0.79
1.75*	0.27	0.33	0.37	1.47	0.79
2.00	0.27	0.32	0.36	1.48	0.78

* Value of d used in the development of the constrained model

TABLE 8

A SUMMARY OF CLASS I DATA EXCLUDED FROM ANALYSIS OF PGA

Description	No. of Events	No. of Recordings	Magnitude Range (M)	Distance* Range (km)	Acceleration Range (g)
Shallow Soil Sites	7	16	5.0-7.1	4-36	.06-.42
Fault Distance Unavailable	11	19	5.0-5.3	2-28**	.02-.35
Pacoima Dam Site, 1971 San Fernando Earthquake-- Extreme Topographic Amplification	1	1	6.6	3.2	1.25
1971 San Fernando Earthquake Data--Excluded from Boore et al. (1980)	1	39	6.6	19-50	.05-.27
Punaluu Site, 1975 Kalapana, Hawaii Earthquake-- Loose Beach Sand	1	1	7.1	27	.11

* Fault Distance

** Epicentral Distance

were found to increase by less than six percent, this accompanied by a ten-percent increase in the standard error and a six-percent decrease in the goodness of fit. The small variation in the predictions is essentially due to the small number of such recordings, since, on the average, observed PGA for the shallow soil sites were found to be 84-percent higher than predicted values based on the other geologic classifications.

San Fernando earthquake data were selected using the criteria set forth by Boore, et al. (1980) in an attempt to minimize the impact of large clusters of predominantly tall buildings in areas such as downtown Los Angeles. We found 39 recordings, excluding the Pacoima Dam record, meeting our selection criteria that were originally excluded from the analysis. We found that by including these data in the analysis, the predictions were essentially unchanged. This is believed to be principally due to the effect of the weighting scheme, which was designed to control the influence of well-recorded earthquakes.

The exclusion of the Pacoima Dam recording* of the 1971 San Fernando earthquake, although justified in a previous section, is relatively controversial, since it represents the largest horizontal peak recordings of acceleration obtained thus far in the world. However, the addition of this station resulted in only a six-percent increase in predicted PGA at eight kilometers for magnitudes of 6.5 to 7.5.

Sensitivity to the exclusion of data for which fault distances were not available is not as straightforward to analyze, since these data could not simply be added to the selected data and the analysis repeated. It was decided that the best analysis would be one in which the observed value of PGA would be compared to predictions based on epicentral distance given by Equation 10. Such a comparison is shown in Figure 10, where the average observed horizontal PGA is plotted versus that predicted by Equation 10.

This figure indicates that the observations are distributed evenly about their median predictions (solid line) and, therefore, are found to be consistent with the rest of the data in the selected data base. Furthermore, we find that seven observations fall outside the plus and minus one-standard-deviation predictions (dashed lines), whereas about six would be expected from a log-normal distribution. This indicates that the scatter in these data are also consistent with that represented by the selected data base. Therefore, we conclude that the inclusion of these data would probably have a negligible effect on the results of this study.

The effect of excluding the Punaluu, Hawaii recording from the analysis was not studied. This recording is low with respect to its prediction based on the unconstrained and constrained models. However, since it represents only one recording, no significant reduction in the median predictions of PGA would be expected if it were included.

* We have shown in a previous section that the recorded value of 1.25 g at the Pacoima Dam station is consistent with our predictions when empirical adjustments for the unusual site conditions at this station are applied.

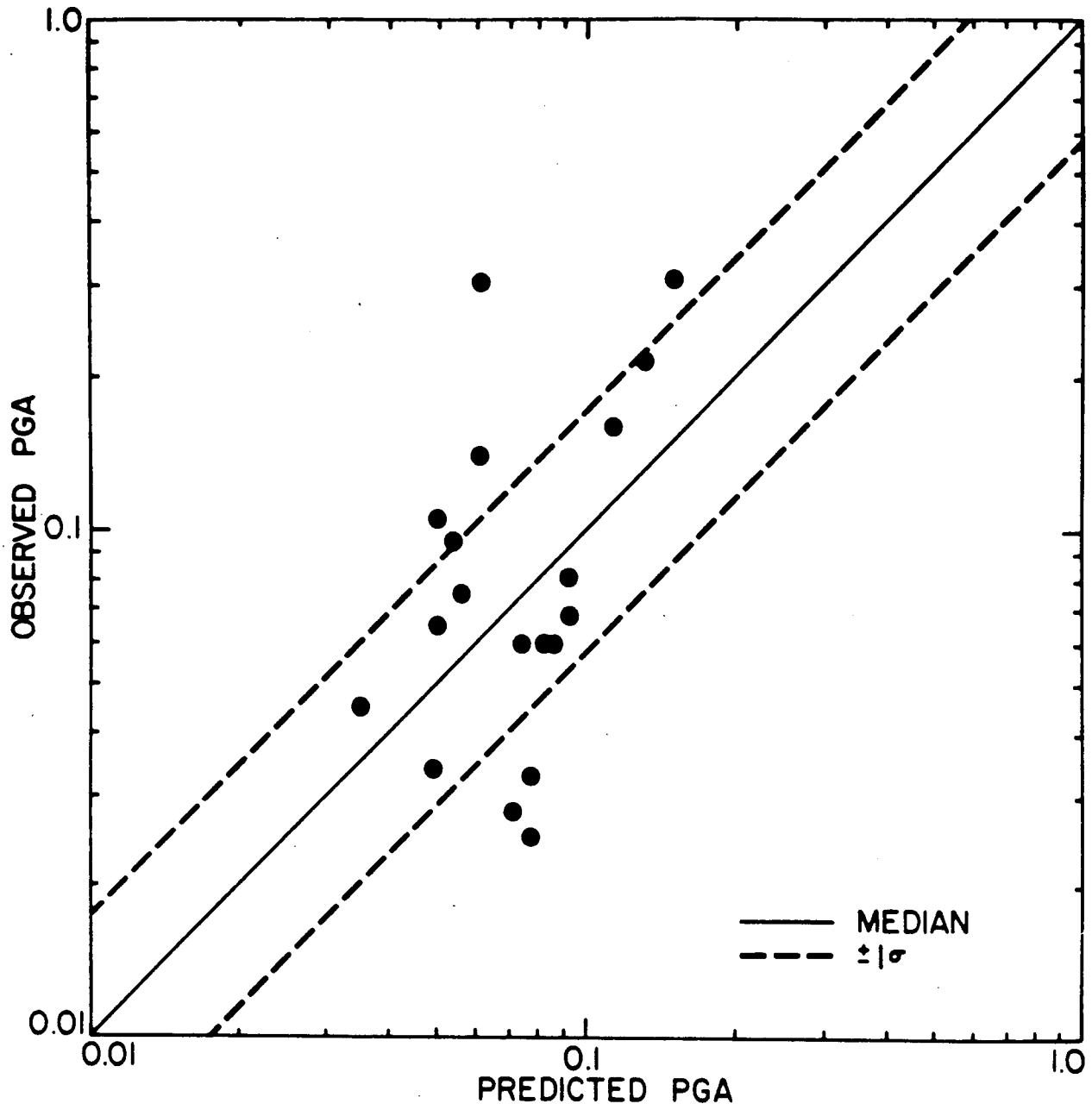


Figure 10. A comparison of observed versus predicted peak accelerations for excluded Class I data with unknown fault distance.

Class II Data: These data, summarized in Table 9, are primarily composed of older recordings obtained from 1933 through 1967. They were excluded from the near-source data base for such reasons as imprecise magnitude determinations, late instrument triggering, inaccurate locations, and undeterminable fault distances. Further discussion is presented below.

The triggering mechanism of the older USGS strong-motion instruments caused relatively large trigger delays with the result that many of the older near-source recordings begin well within the strong phase of shaking. This, of course, results in unreliable estimates of peak acceleration from these recordings and would tend to underestimate the actual PGA.

Due to limited distribution of local seismometer networks in southern and northern California prior to a few decades ago, magnitude determinations generally were reported to the nearest one-half magnitude unit, which by our criteria represents an unacceptable level of uncertainty. The lack of an adequate distribution of seismometers also resulted in errors in epicentral locations of 15 kilometers or greater for certain older earthquakes. Most often, focal depths could not be sufficiently determined from these data and were therefore constrained to 16 kilometers in order to determine the epicenter. Such errors are unacceptably large for meaningful analyses of peak accelerations within 30 or 50 kilometers of the source, and therefore, these data were not used in our near-source studies. Furthermore, the unavailability of aftershock data of sufficient quality and completeness precluded the determination of fault distances for many of these older recordings.

In addition, three recent earthquakes were excluded from analysis. One was excluded because the accuracy of the location was unknown. The other two were excluded because in one case the largest component was less than 0.02 g, and in the other case, both components were less than 0.05 g, their actual values being unknown.

Class II data were analyzed in a manner similar to the Class I data for which significant distances were not available. The mean observed horizontal PGA was compared to that predicted by Equation 10 based on epicentral distance. This comparison is shown in Figure 11. Although we find the observations to be distributed fairly evenly about the median predictions (solid line), twice as many fall below the minus one-standard-deviation prediction than above the plus one-standard-deviation level (dashed lines). Furthermore, one would expect ten values to fall outside these limits assuming a log-normal distribution of PGA, whereas 16 are observed. The bias, then, appears to be associated with lower than average observed accelerations and increased scatter in the observations as was originally expected.

We may conclude from this comparison that median predictions would probably not be affected substantially by including Class II data in the analyses. If any effect is expected, it would probably be to lower the median predictions somewhat. It would appear, however, that the uncertainty in these predictions would be increased by including these data, widening the standard error bounds.

TABLE 9

A SUMMARY OF CLASS II DATA EXCLUDED FROM ANALYSIS OF PGA

Description	No. of Events	No. of Recordings	Magnitude Range (M)	Distance* Range (km)	Acceleration Range (g)
Inaccurate Location; Late Trigger; Imprecise Magnitude; No Fault Distance	25	28	5.0-7.1	6-66	.01-.31
Quality Unknown	1	1	5.0	26	.04
PGA Unknown (<.05 g)	1	1	5.2	13	--
PGA Less Than .02 g	1	1	5.2	17**	.01

* Epicentral Distance

** Fault Distance

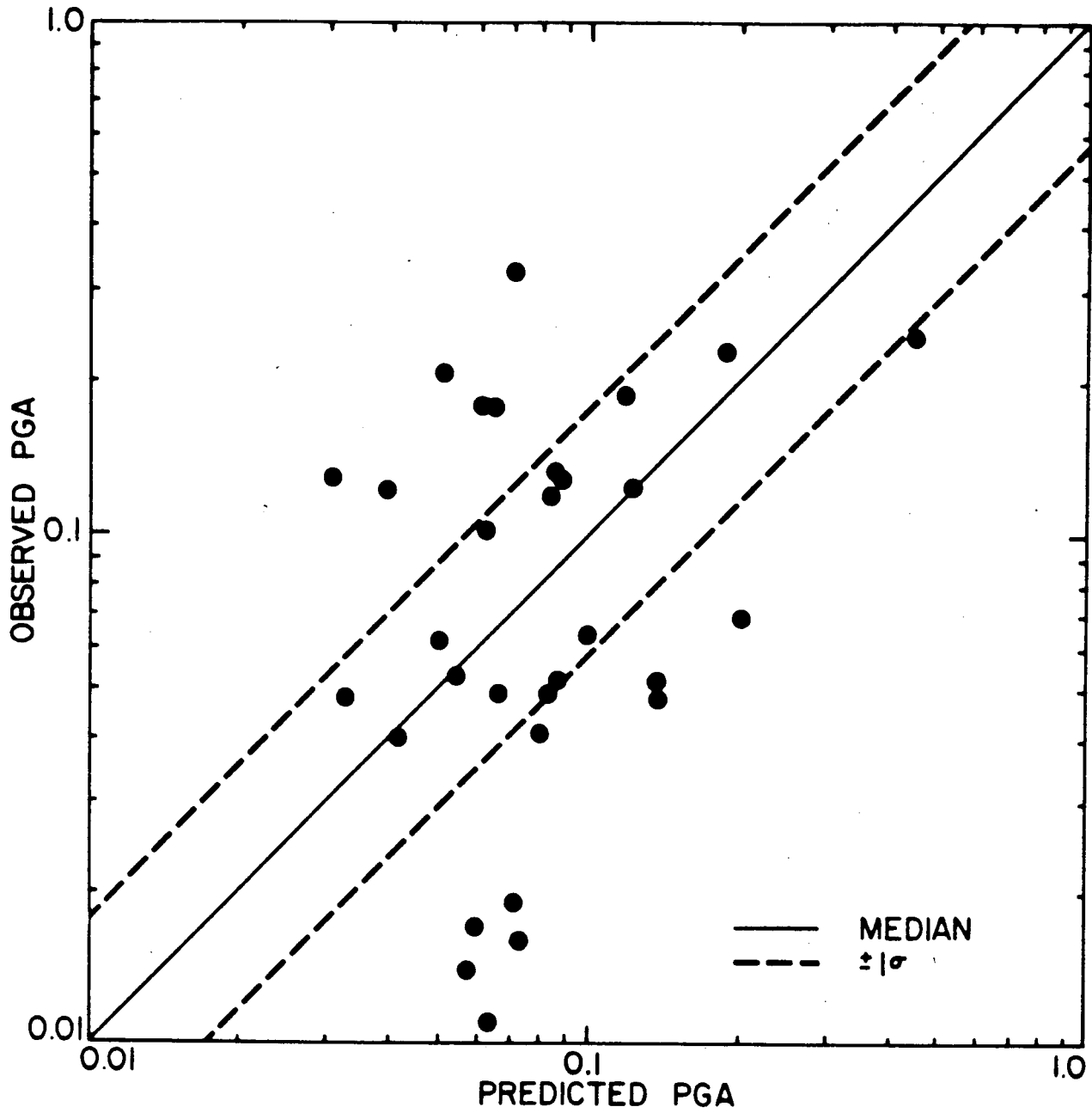


Figure 11. A comparison of observed versus predicted peak accelerations for excluded Class II data with unknown fault distance.

The SAGO Central site (PGA < 0.02 g) from the 1974 Hollister earthquake was the only recording that would normally have been included in the selected data had its PGA been larger. Therefore, it was also compared to predictions based on the unconstrained and constrained models. We found, as expected, that its observed PGA falls substantially below its expected value.

In summary, we believe that the exclusion of Class I and Class II data in the development of the unconstrained and constrained ground motion models has not substantially biased the median predictions of PGA. Rather, their exclusion appears to have reduced the uncertainty associated with these predictions, in accordance with the intent of the selection criteria.

Fault Distance

The shortest distance between the recording station and the fault rupture surface was used in the analyses because it is believed to be a more physically meaningful representation of the travel path of the high-frequency components of strong ground motion than either epicentral or hypocentral distance. To test this hypothesis statistically, the regression analyses described in the section on the ground motion model were repeated using epicentral and hypocentral distances. Since the distribution of data throughout the distance ranges defined in Table 3 varied substantially depending on the distance parameter specified, a single weighting scheme would not be appropriate for all three analyses. Therefore, we decided to perform unweighted analyses for the sake of comparison, and statistical parameters were compared with those for an unweighted regression on fault distance.

This analysis resulted in the following expressions for the median value of PGA:

For epicentral distance (R_e),

$$\text{PGA} = 0.756 \exp(.979M) (R_e + 32.1)^{-1.92} \quad (10)$$

For hypocentral distance (R_h),

$$\text{PGA} = 0.0554 \exp(.988M) (R_h + 11.4)^{-1.43} \quad (11)$$

In each analysis the coefficient c_2 was found to be equal to zero and, therefore, is not included in the above expressions. Both equations are represented by a standard error corresponding to a multiplicative factor of 1.67 and an r-square value of 0.57. This corresponds to a 33-percent increase in the standard error and a 27-percent decrease in the r-square (i.e., goodness of fit) as compared to the unweighted, unconstrained model. An F-test on the ratio of the mean square errors confirmed that the increase in the variances are statistically significant at a greater than 99-percent level of confidence.

A similar analysis was performed for the 1979 Imperial Valley earthquake (M_s 6.9) using data recorded within 50 kilometers of the fault (see Appendix). This event produced the most extensive set of strong-motion recordings within 20 kilometers of the fault rupture surface of any earthquake in history. As with

the entire data base, replacing fault distance by epicentral distance for the Imperial Valley data substantially worsened the fit, creating a 13-percent increase in the standard error and a similar decrease in the goodness of fit.

We conclude, therefore, that the expressions relating PGA to either epicentral or hypocentral distance are statistically inferior to those based on fault distance for near-source data. Therefore, fault distance is believed to represent a more consistent and meaningful definition of distance in the near-source region of moderate-to-large earthquakes than either epicentral or hypocentral distance.

Large Structures

In the analysis of building effects we found that large embedded structures had significantly smaller recorded PGA than small, non-embedded buildings.

In order to assess the effects this may have on the development of the unconstrained model, we extracted from the selected data all data recorded either in the free field or in small buildings (1 to 2 stories) representing 81 recordings from 23 earthquakes. The weighted regression analysis, fitting all coefficients in the ground motion model, yielded the following expression:

$$\text{PGA} = 0.0109 \exp(.994 M) [R + 0.0491 \exp(.771 M)]^{-1.19} \quad (12)$$

The median plus one-standard-deviation value of PGA may be obtained by multiplying the median value by a factor of 1.44. The goodness of fit is represented by an r-square value of 0.82. Both of these values indicate a slightly better fit than was obtained in the unconstrained model which included large buildings.

Although the coefficients in the above expression are somewhat different than in Equation 3, the predicted values of PGA at a distance of five kilometers or greater were found to be essentially identical. This confirms the validity of our results for representing free-field predictions of peak horizontal accelerations. However, the elimination of the large structures from the data base was found to affect magnitude scaling at very short distances (less than five kilometers). For instance, it was found that Equation 12 comes 50-percent closer to supporting magnitude-independence of PGA at the fault rupture surface than the unconstrained model.

Definition of PGA

In essence the use of both horizontal components by most investigators in the development of ground motion models has resulted in the prediction of the mean of the two horizontal components of peak ground acceleration (hereafter referred to as mean PGA). Although unbiased estimates of this mean PGA are obtained in such an analysis, the inclusion of both components as independent data points when in fact they are correlated affects the statistics of the regression analysis. To study this effect the regression analyses resulting in Equations 3 and 5 were repeated using both horizontal components.

As expected, the use of the mean PGA was found to give median predictions of PGA that did not differ from those developed from both components. On the contrary the statistics of the regression analysis were found to vary significantly from the previous analyses. This is explained by the substantial increase in the number of data points and the increased scatter inherent in replacing the mean PGA by its two components. The most significant differences were found in (1) the standard error and goodness-of-fit parameters and (2) the statistical tests of significance.

By using both components of PGA, the standard deviation of the residuals was found to increase by nine percent. This would result in a median plus one-standard-deviation value of PGA that is 1.50 times the median for the unconstrained model and 1.52 times the median for the constrained model. The goodness-of-fit (r-square) was found to decrease by about four percent.

Statistical tests used to test for significant differences in the mean residual between a subset (e.g., geologic classification, fault-type classification, etc.) and the entire data set were found in some cases to result in different conclusions regarding the significance of observed differences when both components were used. The arbitrary increase in the number of points made it less difficult to reject the hypothesis that the mean residual of a subset was no different than that for the entire data set. In other words, the test allows smaller observed differences in order to reject the hypothesis at a specified level of confidence.

Regression analyses on each individual peak horizontal component were associated with standard errors and goodness-of-fit parameters between those obtained for both horizontal components and for mean PGA. The reduction in scatter associated with mean PGA as compared to that obtained for either horizontal component can probably be attributed to an averaging of azimuthal differences between components, which is associated with the random nature of their orientation, among the various recording stations and earthquakes used in the study.

DISCUSSION

The near-source data compiled for this study, of which most have become available only within the last several years, have served as a basis for empirically establishing PGA behavior near a fault. The mathematical relationship used to model this behavior (Equations 1 and 2) was chosen to accommodate any differences in distance and magnitude scaling in the near field required by the data. Physical insight into the observed near-field behavior of PGA is best accomplished from an investigation of the function $C(M)$.

The value of $C(M)$ determines the distance range for which the transition from near-field to far-field attenuation occurs. The tendency for less attenuation of PGA in the near field for values of $C(M)$ greater than zero, which lead to finite values of PGA at the source, is what we define as distance saturation in this

study. Empirical justification for distance saturation comes from both the 1979 Imperial Valley (IV-79) earthquake and the near-source data compiled for this study.

The IV-79 data, plotted in Figure 12, show a definite trend in support of the saturation of PGA at small distances. To quantify this we performed a regression analysis on the IV-79 horizontal accelerations, including data as far as 100 kilometers from the fault in order to empirically constrain the far-field attenuation rate. For this purpose the functional forms given by Equations 1 and 2 were used, where the magnitude coefficients, b and c_2 , were set equal to zero to reflect the attenuation for a specific earthquake. This analysis resulted in a C-value of 20 kilometers and a far-field geometrical attenuation rate $d = -1.77$, values consistent with those found for the constrained ground motion model, Equation 5. The relationship developed from this analysis appears in Figure 12 as the solid curve, with the dashed lines representing the one-standard error bounds.

Values of $C(M)$ for the unconstrained and constrained scaling relationships were found to be magnitude-dependent. These values, given in Table 10, are found to be substantially greater than zero, further supporting distance saturation of PGA in the near field. The sensitivity of these results to the IV-79 data was studied by removing this event and repeating the analyses. The values of $C(M)$ obtained from this analysis are compared with those obtained by including the IV-79 data in Table 10. The similarity in these values confirms the tendency for all near-source data to support the saturation of PGA with distance; the 1979 Imperial Valley earthquake is not unique in this respect.

The differences in the numerical values of $C(M)$ between the constrained and unconstrained ground motion models were found to be a result of the differences in their far-field attenuation rates. These rates required that PGA be proportional to $R^{-1.09}$ in the unconstrained relationship and to $R^{-1.75}$ for the constrained model. The larger attenuation rate, assumed for the latter model in order to make it compatible with other far-field studies, resulted in larger $C(M)$ values in order to accommodate the distance saturation effects required by the near-source data. The similarity between the value of $C(M)$ obtained for the IV-79 event and that computed from the constrained model ($C(M) = 23$ kilometers for $M_s 6.9$) is consistent with this finding since the far-field attenuation rate of these two relationships were found to be virtually identical.

The statistical significance of the observed distance saturation characteristics of PGA was studied by standard hypothesis testing techniques (Bowker and Liebermann, 1972). To isolate these characteristics from any magnitude saturation characteristics, a relationship constraining $C(M)$ to be independent of magnitude was developed and tested. A statistical analysis of the value of C given by this relationship found it to be significantly greater than zero at a level of confidence exceeding 99 percent. A second analysis compared the variance obtained from this constant- C model with another model where $C(M)$ was constrained to a value of zero, thereby eliminating any distance saturation. An F-test found the variance associated with this zero- C model to be significantly greater than the variance of the constant- C relationship at a 95-percent level of

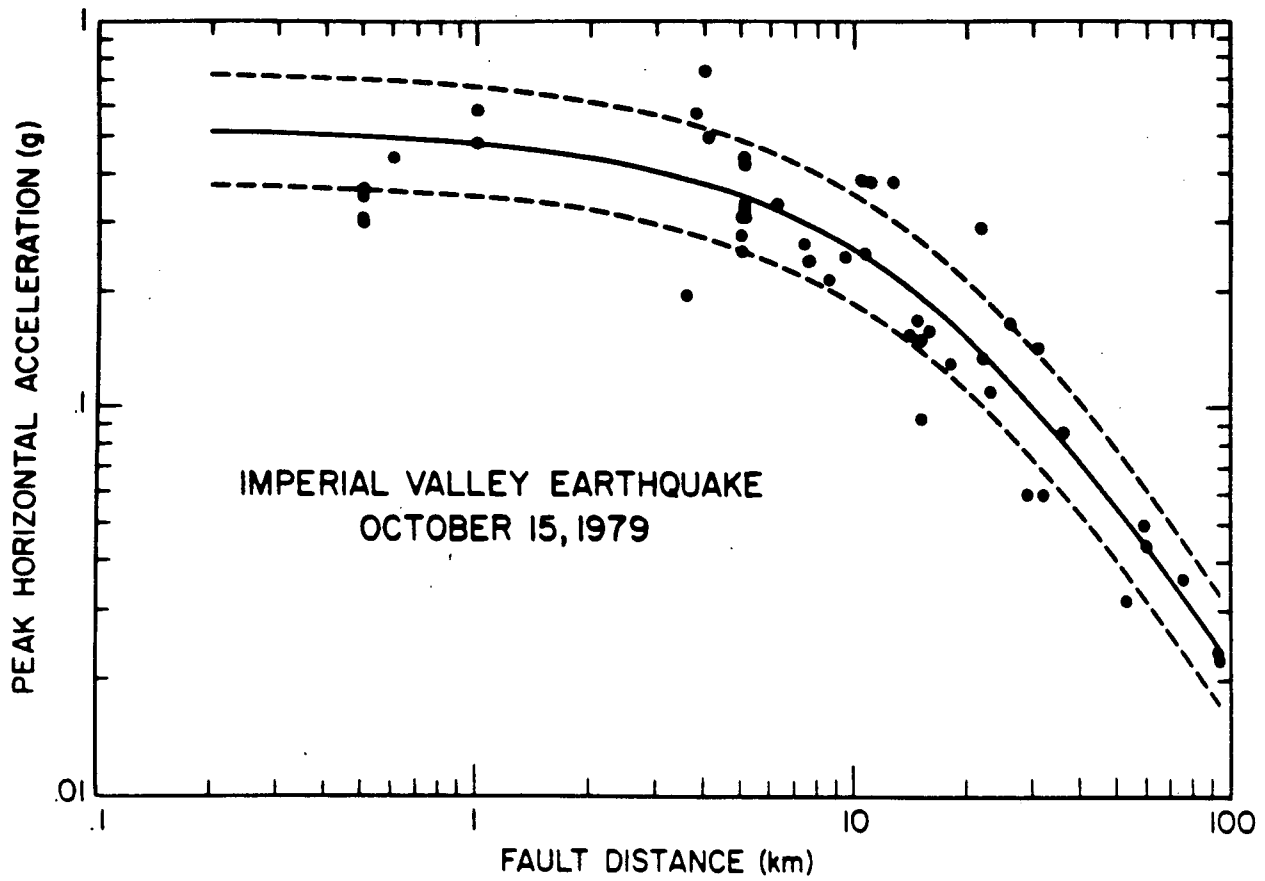


TABLE 10
 DISTANCE SATURATION CHARACTERISTICS
 OF NEAR-SOURCE ACCELERATIONS

Ground Motion Model	M	C(M) (kilometers)
<u>Unconstrained</u>		
Including 1979 Imperial Valley Earthquake	5.5	3
	6.5	6
	7.5	12
Excluding 1979 Imperial Valley Earthquake	5.5	3
	6.5	6
	7.5	11
<u>Constrained</u>		
Including 1979 Imperial Valley Earthquake	5.5	8
	6.5	17
	7.5	36
Excluding 1979 Imperial Valley Earthquake	5.5	7
	6.5	16
	7.5	37

confidence. Therefore, both tests statistically confirmed the importance of distance saturation in modeling the near-source attenuation of peak acceleration.

The exponential function of magnitude adopted for $C(M)$ was designed to accommodate possible variations in magnitude scaling with distance. Values of c_2 greater than zero indicate less dependence on magnitude as distance becomes smaller. This characteristic of PGA we define as magnitude saturation, with total saturation referring to a constant value of PGA at the fault rupture surface.

The degree to which magnitude saturation is supported by the data may be conveniently expressed by a parameter referred to as the degree of magnitude saturation (DMS) which is defined as

$$DMS = \frac{c_2 d}{b} \times 100 \quad (13)$$

where the terms on the right-hand side of the expression represent coefficients of the ground motion model defined in Equations 1 and 2. When $DMS = 0\%$ ($c_2 = 0$), the model predicts constant magnitude scaling at all distances, thereby rejecting magnitude saturation effects. When $DMS = 100\%$ ($c_2 = b/d$), the model predicts a reduction in magnitude scaling with decreasing distance leading to total magnitude saturation at the fault rupture surface. This latter constraint was used in the development of Equation 5.

The degree to which the near-source data support magnitude saturation was found to be influenced by the presence of large structures and by the rupture mechanism of the earthquakes. The results of this study appear in Table II. The unconstrained model was found to support an 88-percent degree of magnitude saturation without any regard to building or fault-type effects. When large buildings (number of stories greater than two) were removed, this value increased to 93 percent. When reverse-fault biases were accounted for through a scaling variable, the data were found to support total magnitude saturation at the fault rupture surface consistent with the assumption used to develop the constrained model. Therefore, near-source data are found to support the saturation of peak acceleration with magnitude.

The statistical significance of the magnitude saturation characteristics of PGA comes from an analysis of the coefficient c_2 which determines the magnitude dependence of $C(M)$. Statistical analysis found c_2 to be significantly greater than zero at levels of confidence exceeding 99 percent (Table II). This value is significantly higher than the traditional 90-percent confidence test and establishes the importance of magnitude saturation effects in modeling the near-source behavior of PGA.

Additional statistical support is reflected in the level of confidence in the observed differences between the variances of each model listed in Table II and that of the constant-C model described previously. The constant-C model, while accommodating distance saturation, was constrained to exclude any magnitude

TABLE II
MAGNITUDE SATURATION CHARACTERISTICS
OF NEAR-SOURCE ACCELERATIONS

Structure Size	Fault-Type Scaling Variable	Degree of Magnitude Saturation	Confidence Level	
			Reduction in Variance	coefficient c_2
All Sizes	Not Included	88%	61%	>99%
Small	Not Included	93%	69%	>99%
Small	Included	100%	75%	>99%

saturation effects. As seen in Table II, the highest level of confidence determined from an F-test, which corresponded to a 14-percent reduction in the variance, comes from the model that excludes large structures and provided for scaling by fault type. Although not passing the traditional 90-percent confidence test, the computed value of 75 percent demonstrates a relatively significant reduction in the variance. With the amount of scatter inherent to peak acceleration data, confidence levels much higher than 75 percent are probably not possible until more data within five kilometers or so from the fault rupture surface become available.

Independent justification of magnitude and distance saturation of peak acceleration in the near field comes from the earthquake modeling studies of Del Mar Technical Associates (1979) and Hadley and Helmberger (1980). They used numerical modeling techniques to simulate the complex physical processes that would occur during moderate-to-large earthquakes in the hopes of gaining an understanding of the behavior of the high frequency components of ground motion near a fault. They found peak accelerations scaled from their simulated accelerograms to become independent of both magnitude and distance in the near field in support of saturation. In particular, Hadley and Helmberger (1980) suggest from their results that empirical attenuation relationships of the form $PGA \propto (R+C)^{-d}$ as used in this study should incorporate a magnitude-dependent function of C in order to account for this near-field behavior. Therefore, we may conclude that the near-source behavior of peak acceleration empirically predicted by our relationships is consistent with physical earthquake processes.

The sensitivity of our predictions to various assumptions used in the development of the ground motion models was studied to test the reliability of these relationships. As described previously, these studies included the effect of model variations, far-field attenuation rate, parameter definitions, and data selection criteria. Near-field predictions of acceleration based on these studies were found to fall well within the one-standard error bounds of Equations 3 and 5 with variations generally less than five to ten percent. Of particular interest was the similarity in the predictions given by the ground motion models used in this study with predictions based on identical analyses using our data and the mathematical form of the relationships proposed by Donovan and Bornstein (1978) and Joyner and Boore (1981). In the latter analysis, our data were found to statistically support an exponential function of magnitude for the depth coefficient h , as defined by the investigators of that study, reflecting the significant magnitude saturation characteristics of these near-source data.

Data from the United States that were excluded from the analysis for reasons other than their failure to meet magnitude and distance constraints were studied to assess their potential impact on the results. They were compared either to predictions based on Equation 3 if fault distance was known or to predictions based on epicentral distance if fault distance was not known. This comparison found the excluded data to be generally consistent with the median estimates of PGA but demonstrating a larger degree of scatter. Therefore, their exclusion apparently has not systematically biased the estimates but rather has reduced the uncertainty associated with these predictions in accordance with the intent of the selection criteria.

Our ground motion models may be compared with a recent study by Joyner and Boore (1981) who used both recently available near-source data and far-field data to establish a relationship for the scaling of peak horizontal acceleration as a function of moment magnitude (Kanamori and Hanks, 1979) and closest distance from the surface projection of the fault rupture surface. Predictions based on their relationship are compared to those given by the unconstrained attenuation model (Equation 3) in Figure 13. Since their analysis used only the maximum horizontal component of peak acceleration, their values were reduced by 12 percent so they could be directly compared to our predictions of mean peak horizontal acceleration.

Inspection of Figure 13 finds their predicted values to deviate from ours by generally less than one-half of a standard error, relatively good agreement considering the differences in the data sets. Only slight differences in the shape of the curves at distances less than 50 kilometers result from the difference in the functional form of their distance term. Their distance term is defined as the square root of the sum of squares of distance and a depth term, and causes the transition from near-field attenuation to far-field attenuation to occur more abruptly than does our distance term.

The largest difference in the two relationships is in the amount of magnitude scaling at distances less than about 10 kilometers. The Joyner and Boore (1981) relationship provides for constant magnitude scaling at all distances (0-200 kilometers), independent of magnitude, corresponding to a 77-percent increase in peak acceleration per magnitude unit. Our data, on the other hand, supported reduced magnitude scaling in the near field, the amount of the reduction being dependent on the size of the event. Our relationship gives a 114-percent increase in peak acceleration from M6.5 to M7.5 at 50 kilometers, decreasing to a 48-percent increase for the same magnitude interval at a distance of five kilometers.

A thorough understanding of the differences in magnitude scaling between the two relationships would require a detailed comparison of the data sets and statistical techniques used in each analysis which is beyond the scope of this study. As suggested by Joyner and Boore (1981), part of the difference may be due to their definition of distance. Their use of closest distance to the surface projection of the fault rupture surface would give smaller distances than would our definition for the smaller magnitude events not accompanied by surface rupture. As a result, their data would be expected to support a larger degree of magnitude scaling between moderate and large earthquakes in the near field. For earthquakes exceeding magnitudes 6.0 to 6.3, which generally rupture to the ground surface, their definition of distance becomes consistent with ours and might then be expected to support reduced magnitude scaling in the near field. To understand the effect of distance definition on the near-source behavior of PGA, we developed a ground motion model from our data, using closest distance to the surface projection of the fault rupture zone, and compared it to the unconstrained relationship given by Equation 3. As expected, we found that by using this alternate distance definition the degree of magnitude saturation decreased, whereby magnitude scaling within ten kilometers of the fault increased for the smaller magnitude earthquakes. However, we find that both the predictions and magnitude scaling of peak acceleration for the larger events

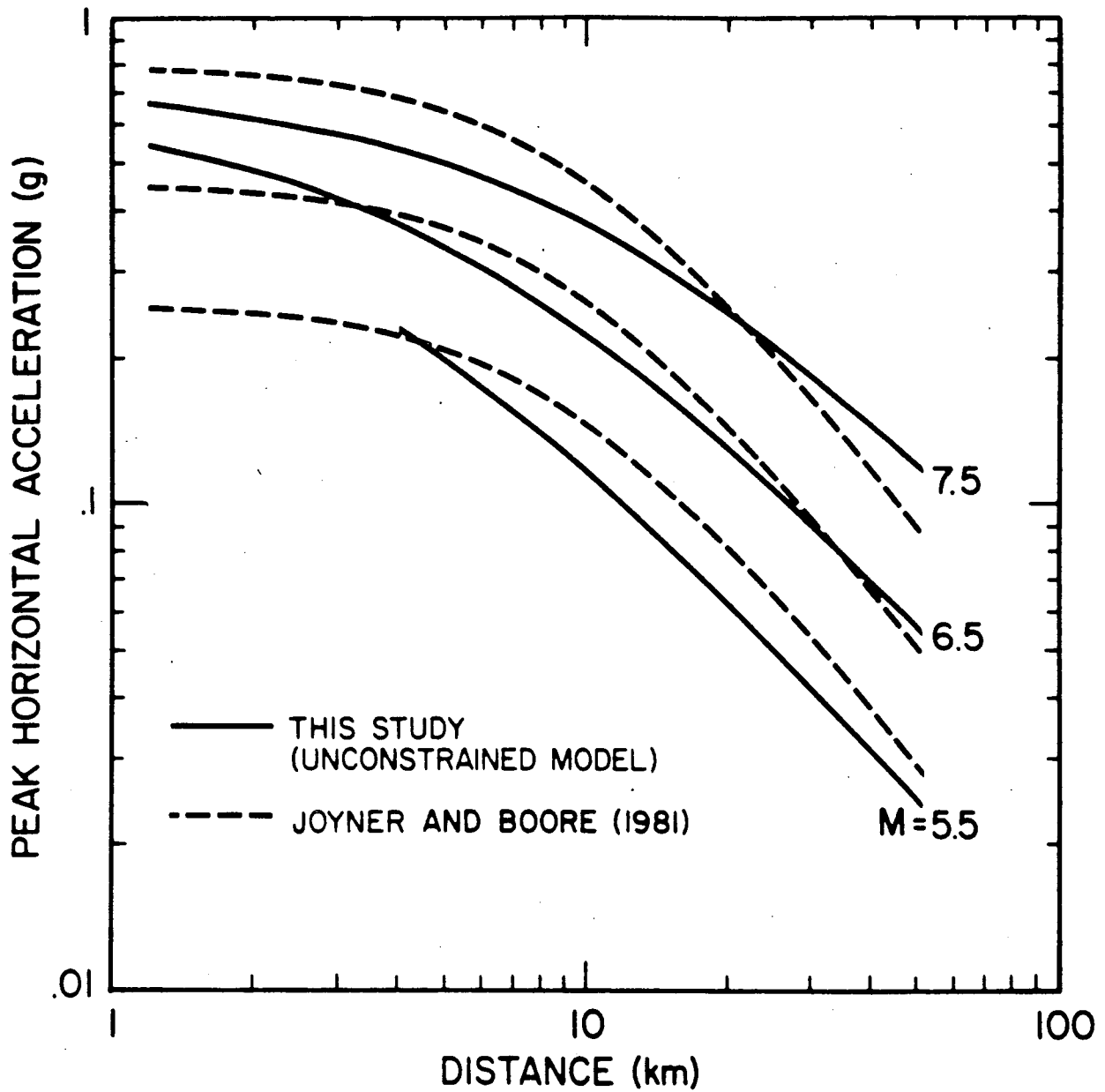


Figure 13. The unconstrained ground motion model (solid curve) compared with the attenuation relationship (dashed curve) developed by Joyner and Boore (1981). The Joyner and Boore predictions of the maximum horizontal component have been reduced by 12 percent so that they may be compared with the predictions of the mean horizontal peak acceleration given by the unconstrained model.

remained the same. Although the physically-based concept of total magnitude saturation at zero distance is no longer appropriate for the smaller events using this alternate distance definition, it is important that reduced magnitude scaling for the larger events continued to be statistically supported by our near-source data strengthening our conclusions regarding the near-source behavior of peak acceleration. Therefore, we conclude that differences in analysis techniques and data selection criteria must be responsible for differences in predicted magnitude scaling characteristics between the two studies.

CONCLUSIONS

Based upon the results of the analyses, the sensitivity studies, and the discussions presented in this report, we offer the following conclusions with regard to the characteristics of horizontal peak ground acceleration (PGA) recorded in the near-source region of moderate to large earthquakes:

- o The results of this study have established that accelerations tend to saturate with increasing magnitude at small distances. Conclusions regarding magnitude saturation of PGA were found to be influenced by the effects of fault type and building size. When the analysis was restricted to small structures and fault type was treated as a variable, the unconstrained model was found to support complete saturation of PGA at the fault rupture surface, consistent with the assumption used in the development of the constrained model.
- o Both the 1979 Imperial Valley earthquake data and the results of this study were found to support saturation of acceleration with decreasing distance. This confirms the inappropriateness of a linear extrapolation of far-field data in estimating near-source accelerations.
- o Based on the data compiled for this study, there was found to be no significant difference between accelerations recorded on rock or soil once shallow soil sites were removed. PGA from shallow soil sites were found to be 63- to 84-percent higher than those from either soil or rock sites.
- o A 24-percent reduction in PGA was found to exist for recordings obtained in the basement of large buildings, when compared to ground-level recordings in small (1- and 2-story) buildings or in the free field.
- o An extensive sensitivity analysis has established the robustness of the PGA ground motion models developed in this study. Predicted accelerations for variations in parameter values, ground motion models and data selection criteria were found to fall well within the one-standard-deviation estimates given by the unconstrained and constrained models, their variations being generally less than five to ten percent.

- o Sensitivity studies confirmed the adequacy of the weighting scheme in controlling the effect of well-recorded events. The chosen scheme was found to represent a reasonable balance between the contributions to distance attenuation inherent in well-recorded earthquakes and the contributions to magnitude scaling, especially at small distances, offered by significant but more poorly recorded events.
- o Non-North American accelerations, primarily from reverse-type faults, were found to be systematically high relative to the primarily strike-slip North American data. Reverse-fault data were found to be 17- to 28- percent higher than data from other fault types.
- o Accelerations recorded at sites located within areas of steep topographic relief were found to be significantly higher than the average. The Pacoima Dam accelerations recorded during the 1971 San Fernando earthquake are found to be consistent with those predicted by the unconstrained model when empirically-derived corrections for topography, site conditions, response of the dam, and fault type are accounted for.
- o A comparative analysis of several distance definitions found ground motion models based on fault distance, as defined in this study, to be far superior to those based on either epicentral or hypocentral distance. Use of these latter distance definitions resulted in a 33-percent increase in the scatter and a 27-percent decrease in the goodness of fit.
- o Data from the United States that were excluded based on the selection criteria set forth in this study were not found to vary systematically from their predicted values. Rather, their exclusion has reduced the uncertainty associated with these predictions in accordance with the intent of the selection criteria.
- o The results from the constrained model for very small distances were found to be insensitive to the specified far-field acceleration attenuation rate over the range 1.0 to 2.0. Separate application of the near-field and far-field constraints used in the development of the constrained model yielded predictions relatively consistent with the unconstrained model.
- o Statistical assumptions regarding the lognormal distribution of PGA were confirmed, verifying the use of various statistical tests employed throughout the analyses that required this assumption.

The sensitivity studies described in this report confirm the appropriateness of using the ground motion models given by Equations 3 and 5 for the prediction of peak horizontal acceleration at SONGS for the reasons summarized below:

- o The emphasis on the near-source region of moderate-to-large earthquakes is consistent with the design earthquake, an M_s 7.0 event located 8 kilometers from SONGS on the Offshore Zone of Deformation.
- o Our predictions are representative of free-field conditions, being based on strong-motion data predominantly recorded at ground level in instrument shelters or small buildings.
- o Our predictions are valid for both soil and rock, provided the site is not located on shallow soil deposits less than 10 meters thick, whereas the dynamic characteristics of the SONGS site would indicate that it should be classified somewhere between a soft rock and a very stiff, deep soil.
- o Although reverse fault data were included in the development of the ground motion models, our analyses confirmed that their presence would tend to result in larger predicted values of PGA than if only strike-slip faulting mechanisms, appropriate for the OZD, had been included.

From our studies, we find that predictions at SONGS based on the unconstrained model are 0.33 g and 0.48 g for the median and 84th-percentile values of peak horizontal acceleration, respectively, and those based on the constrained model are 0.32 g and 0.47 g. If scatter associated with both horizontal components rather than the mean of the two horizontal components is used, then the 84th percentile values increase to 0.50 g and 0.49 g for the unconstrained and constrained models respectively. The predictions were found to be very stable with respect to reasonable model and parameter variations.

REFERENCES

- Aki, K., and P. Richards (1980), "Quantitative Seismology Theory and Methods," Vol. II, W.H. Freeman and Company, San Francisco.
- Ambraseys, N.N. (1969), "Maximum Intensity of Ground Movements Caused by Faulting," Proc. Fourth World Conf. Earthquake Engr., Santiago, Chile, Vol. I, pp. 154-171.
- Ambraseys, N.N. (1973), "Dynamics and Response of Foundation Materials in Epicentral Regions of Strong Earthquakes," Proc. Fifth World Conf. Earthquake Engr., Rome, Italy, Vol. I, pp. 126-148.

- Ambraseys, N.N. (1978), "Preliminary Analysis of European Strong-Motion Data 1965-1978," *Bulletin of European Assoc. for Earthquake Engineers*, 4:17-37.
- Bolt, Bruce A. (1978), "Fallacies in Current Ground Motion Prediction," *Proc. Second Int'l Conf. on Microzonation, San Francisco, California, Vol. II*, pp. 617-633.
- Boore, D.M. (1973), "The Effect of Simple Topography on Seismic Waves: Implications for the Accelerations Recorded at Pacoima Dam, San Fernando Valley, California," *Bull. Seism. Soc. Am.*, 63:1603-1609.
- Boore, D.M., W.B. Joyner, A.A. Oliver III and R.A. Page (1980), "Peak Acceleration, Velocity, and Displacement from Strong-Motion Records," *Bull. Seism. Soc. Am.*, 70(1):305-321.
- Bowker, A.H. and G. J. Liebermann (1972), "Engineering Statistics," Prentice-Hall, Inc., Englewood Cliffs, New Jersey.
- Brune, J.N. (1970), "Tectonic Stress and the Spectra of Seismic Shear Waves from Earthquakes," *J. Geophys. Res.*, 75(26):4997-5009.
- Campbell, Kenneth W. (1980), "Attenuation of Peak Horizontal Acceleration Within the Near-Source Region of Moderate to Large Earthquakes," TERA Corporation Technical Report 80-1, Berkeley, California.
- Chinnery, Michael A. (1978), "Measurement of m_b with a Global Network," *Tectonophysics*, 49:139-144.
- Crouse, C.B. (1978), "Prediction of Free-Field Earthquake Ground Motions," *Proceedings of Specialty Conference on Earthquake Engineering and Soil Dynamics, ASCE, Pasadena, California, Vol. I*, pp. 359-379.
- Darragh, R.B. and K.W. Campbell (1981), "Empirical Assessment of the Reduction in Free Field Ground Motion Due to the Presence of Structures," (abstract), *Earthquake Notes*, 52(1):18.
- Del Mar Technical Associates (1979), "Simulation of Earthquake Ground Motions for San Onofre Nuclear Generating Station Unit I, Supplement I," Del Mar Technical Associates Report to Southern California Edison Company, Del Mar, California.
- Dietrich, J.H. (1973), "A Deterministic Near-Field Source Model," *Proc. Fifth World Conf. Earthquake Engr.*, Rome, Italy, Paper 301.
- Donovan, N.C., and A.E. Bornstein (1978), "Uncertainties in Seismic Risk Procedures," *Journal of the Geotechnical Engineering Division, ASCE*, 104 (GT7):869-887.

- Duke, C. M., J. A. Johnson, Y. Kharraz, K. W. Campbell, and N. A. Malpiede (1971), "Subsurface Site Conditions and Geology in the San Fernando Earthquake Area," School of Engineering and Applied Science Report UCLA-ENG-7206, University of California, Los Angeles.
- Esteva, Luis (1970), "Seismic Risk and Seismic Design Criteria for Nuclear Power Plants," The MIT Press (Edited by Robert J. Hansen), Cambridge, Massachusetts, pp. 142-182.
- Gallant, A.R. (1975), "Nonlinear Regression," *The American Statistician*, 29(2): 73-81.
- Hadley, D.M. and D.V. Helmberger (1980), "Simulation of Strong Ground Motions," *Bull. Seism. Soc. Am.*, 70(2):617-630.
- Hanks, T.C. and H. Kanamori (1979), "A Moment Magnitude Scale," *J. Geophys. Res.*, 84: 2348-2350.
- Hanks, T.C. and D.A. Johnson (1976), "Geophysical Assessment of Peak Accelerations," *Bull. Seism. Soc. Am.*, 66:959-968.
- Hanks, T.C. (1979), "b Values and ω^{-2} Seismic Source Models: Implications for Tectonic Stress Variations Along Active Crustal Fault Zones and the Estimation of High-Frequency Strong Ground Motion," *J. Geophys. Res.*, 84(B5): 2235-2242.
- Jennings, P.C. and R.A. Guzman (1975), "Seismic Design Criteria for Nuclear Power Plants," Proceedings of U.S. National Conference on Earthquake Engineering, EERI, Ann Arbor, Michigan, pp. 474-483.
- Joyner, W.B. and D.M. Boore (1981), "Peak Horizontal Acceleration and Velocity from Strong-Motion Records Including Records from the 1979 Imperial Valley, California, Earthquake," *Bull. Seism. Soc. Am.*, Vol. 71 (in press).
- Kanamori, Hiroo (1979), "A Semi-Empirical Approach to Prediction of Long-Period Ground Motions from Great Earthquakes," *Bull. Seism. Soc. Am.*, 69(6):1645-1670.
- Krishna, J., A.R. Chandrasekaran, and S.S. Sanai (1969), "Analysis of Koyna Accelerogram of December 11, 1967," *Bull. Seism. Soc. Am.*, 59:1719-1731.
- McGarr, A. (1981), "Analysis of Peak Ground Motion in Terms of a Model of Inhomogeneous Faulting," *J. Geophys. Res.*, 86:3901-3912.
- McGarr, A., R.W.E. Green and S.M. Spottiswoode (1981), "Strong Ground Motion of Mine Tremors: Some Implications for Near-Source Ground Motion Parameters," *Bull. Seism. Soc. Am.*, 71(1): 295-319.
- Mickey, W.V., V. Perez and W.K. Cloud (1973), "Response of Pacoima Dam to Aftershocks of San Fernando Earthquake," in the San Fernando, California, Earthquake of February 9, 1971, EERI/NOAA, Vol. II, pp. 403-415.

- Midorikawa, S. and H. Kabayashi (1978), "On Estimation of Strong Earthquake Motions with Regard to Fault Rupture," Proc. Second Int'l Conf. on Microzonation, San Francisco, California, Vol. II, pp. 825-836.
- Nuttli, O.W. (1979), "The Relations of Sustained Maximum Ground Acceleration and Velocity to Earthquake Intensity and Magnitude," in State-of-the-Art for Assessing Earthquake Hazards in the United States, U.S. Army Engineer Waterways Experiment Station, Vicksburg, Miss., Misc. Paper S-73-1, Report 16.
- Reimer, R.B., R.W. Clough and J.M. Raphael (1973), "Evaluation of the Pacoima Dam Accelerogram," Proc. Fifth World Conf. Earthquake Engr., Rome, Italy, Paper 293.
- Seekins, L.C. and T.C. Hanks (1978), "Strong-Motion Accelerograms of the Oroville Aftershocks and Peak Acceleration Data," Bull. Seism. Soc. Am., 68(3):667-689.
- Trifunac, M.D. (1973), "Analysis of Strong Earthquake Ground Motion," Int. J. Earthq. Engr. Struct. Dyn., 2:59-69.

APPENDIX
STRONG MOTION DATA

EARTHQUAKE NAME	DATE YR-MO-DY	MAGNITUDE ^a (M)	USGS NO.	STATION NAME	FAULT ^b DISTANCE	GEOLOGY ^c CLASS	PEAK GROUND ACCELERATION (g)	
Long Beach	33-03-11	6.2	131	Long Beach Pub Util Bldg	6.4	B	.20	.16
Long Beach	33-03-11	6.2	136	LA Subway Terminal	28.0	C	.098	.064
Long Beach	33-03-11	6.2	288	Vernon CMD Terminal	22.0	A	.15	.13
Helena, Montana	35-10-31	5.5	2229	Helena Mont Fed Bldg	8.0	D	.15	.15
Imperial Valley	40-05-19	7.1	117	El Centro Sta 9	10.0	A	.35	.21
Santa Barbara	41-07-01	5.9	283	Sta Barbara Courthouse	10.0	B	.24	.18
Kern County	52-07-21	7.7	1095	Taft Lincoln School	42.0	A	.197	.177
Daly City	57-03-22	5.3	1049	Oakland City Hall	24.0	B	.047	.029
Daly City	57-03-22	5.3	1065	SF Alexander Bldg	14.0	A	.055	.050
Daly City	57-03-22	5.3	1078	SF So Pacific Bldg	14.0	A	.049	.046
Daly City	57-03-22	5.3	1080	SF State Bldg	12.0	A	.103	.062
Daly City	57-03-22	5.3	1117	SF Golden Gate Park	8.0	C	.126	.105
Parkfield	66-06-28	6.0	1013	Cholame-Shandon Sta 2	0.08	A	.73	.51
Parkfield	66-06-28	6.0	1014	Cholame-Shandon Sta 5	5.5	A	.47	.40
Parkfield	66-06-28	6.0	1015	Cholame-Shandon Sta 7	9.6	B	.28	.27
Parkfield	66-06-28	6.0	1016	Cholame-Shandon Sta 12	14.9	A	.072	.06
Parkfield	66-06-28	6.0	1438	Cholame-Shandon Temblor	10.6	E	.41	.29
Fairbanks, Alaska	67-06-21	5.7	2721	Fairbanks Duck Hall	15.0	D	.14	.09
Koyna, India	67-12-10	6.5	9000	Koyna Dam (Gallery 1A)	3.2	D	.63	.49
Borrego Mtn	68-04-09	6.7	117	El Centro Sta 9	45.0	A	.142	.061
Little Creek	70-09-12	5.4	111	Cedar Sprng Miller Cyn	18.0	D	.086	.059
Little Creek	70-09-12	5.4	113	Colton SCE Substation	29.0	A	.045	.041
Little Creek	70-09-12	5.4	116	Devils Canyon filter plant	19.0	E	.18	.17
Little Creek	70-09-12	5.4	274	Hall of Rcrds San Bern	28.0	A	.12	.06
Little Creek	70-09-12	5.4	278	Puddingstone Reservoir	32.0	C	.022	.02
Little Creek	70-09-12	5.4	290	Wrightwood	15.0	E	.21	.14
Little Creek	70-09-12	5.4	557	Cedar Springs Pump Plant	18.0	E	.073	.062
San Fernando	71-02-09	6.6	104	Santa Anita Dam	27.9	D	.24	.18
San Fernando	71-02-09	6.6	110	Castaic Old Rdg. Rt.	22.8	E	.39	.32
San Fernando	71-02-09	6.6	121	Fairmont Reservoir	32.1	E	.17	.15

APPENDIX

(CONT.)

EARTHQUAKE NAME	DATE YR-MO-DY	MAGNITUDE ^a (M)	USGS NO.	STATION NAME	FAULT ^b DISTANCE	GEOLOGY ^c CLASS	PEAK GROUND ACCELERATION (g)	
San Fernando	71-02-09	6.6	125	Lake Hughes Sta 1	29.6	A	.17	.12
San Fernando	71-02-09	6.6	126	Lake Hughes Sta 4	24.9	E	.19	.16
San Fernando	71-02-09	6.6	127	Lake Hughes Sta 9	22.6	E	.16	.15
San Fernando	71-02-09	6.6	128	Lake Hughes Sta 12	18.7	E	.37	.28
San Fernando	71-02-09	6.6	133	LA Hollywd Storage Bld	21.3	A	.15	.11
San Fernando	71-02-09	6.6	135	LA Hlywd Strge Pl Lot	20.5	A	.22	.19
San Fernando	71-02-09	6.6	137	LA Water and Power	24.1	C	.20	.14
San Fernando	71-02-09	6.6	141	LA Griffith Park Observ	16.9	D	.18	.16
San Fernando	71-02-09	6.6	181	LA 1640 Marengo	25.2	B	.14	.14
San Fernando	71-02-09	6.6	190	LA 2011 Zonal	25.5	C	.08	.07
San Fernando	71-02-09	6.6	220	LA 3838 Lankershim	15.4	C	.18	.13
San Fernando	71-02-09	6.6	229	LA 5250 Century	36.1	B	.06	.06
San Fernando	71-02-09	6.6	241	LA 8244 Orion	7.5	A	.27	.14
San Fernando	71-02-09	6.6	244	LA 8639 Lincoln	36.1	B	.04	.04
San Fernando	71-02-09	6.6	247	LA 9841 Airport Blvd	36.1	B	.03	.03
San Fernando	71-02-09	6.6	253	LA 14724 Ventura	15.4	A	.26	.19
San Fernando	71-02-09	6.6	262	Palmdale Fire Sta	27.6	A	.13	.11
San Fernando	71-02-09	6.6	264	Pasadena Millikan Lib	21.8	B	.21	.18
San Fernando	71-02-09	6.6	266	Pasadena CIT Seismo Lab	18.4	D	.19	.11
San Fernando	71-02-09	6.6	267	Pasadena Jet Prop Lab	14.8	B	.22	.17
San Fernando	71-02-09	6.6	269	Pearblossom Pump Plant	35.5	E	.15	.10
San Fernando	71-02-09	6.6	279	Pacoima Dam	3.2	E	1.25	1.24
San Fernando	71-02-09	6.6	288	Vernon CMD Terminal	30.7	A	.11	.09
San Fernando	71-02-09	6.6	458	LA 15107 Van Owen	9.7	A	.12	.11
San Fernando	71-02-09	6.6	461	LA 15910 Ventura	14.3	A	.15	.13
San Fernando	71-02-09	6.6	466	LA 15250 Ventura	15.4	A	.23	.14
San Fernando	71-02-09	6.6	475	Pasadena Athenaeum Cit	22.5	B	.11	.10
San Fernando	71-02-09	6.6	482	Alhambra 900 S Fremont	24.8	B	.13	.11
Bear Valley	72-02-24	5.1	1028	Hollister City Hall	31.0	A	.03	.02
Sitka, Alaska	72-07-30	7.6	2714	Sitka Alaska Mag Obs	45.0	A	.11	.09

APPENDIX

(CONT.)

EARTHQUAKE NAME	DATE YR-MO-DY	MAGNITUDE ^a (M)	USGS NO.	STATION NAME	FAULT ^b DISTANCE	GEOLOGY ^c CLASS	PEAK GROUND ACCELERATION (g)	
Managua	72-12-23	6.2	3501	Managua Esso Refinery	5.0	A	.39	.34
Point Mugu	73-02-21	5.9	272	Port Hueneke Naval Lab	24.0	A	.13	.08
Lima, Peru	74-10-03	7.6	4302	Lima Geophysical Inst	38.0	B	.24	.21
Lima, Peru	74-10-03	7.6	4304	Lima Huaca Residence	40.0	B	.25	.20
Hollister	74-11-28	5.1	1028	Hollister City Hall	10.8	A	.17	.10
Hollister	74-11-28	5.1	1250	Gilroy Gavilan Col	10.8	B	.14	.10
Hollister	74-11-28	5.1	1377	San Juan Bautista	8.9	A	.12	.05
Oroville	75-08-01	5.7	1051	Oroville Seismo Sta	8.0	D	.11	.10
Oroville	75-08-01	5.7	1291	Marysville	30.0	A	.07	.06
Oroville	75-08-01	5.7	1292	Chico	31.0	A	.08	.06
Oroville	75-08-01	5.7	1293	Paradise KEWG Transmtr	32.0	C	.04	.03
Kalapana, Hawaii	75-11-29	7.1	2803	Panalu, Hawaii	27.0	F	.12	.10
Kalapana, Hawaii	75-11-29	7.1	2808	Hilo, Hawaii	45.0	E	.22	.11
Gazli, USSR	76-05-17	7.0	9110	USSR, Karakyr	3.5	C	.81	.65
Santa Barbara	78-08-13	5.7	106	Cochuma Dam Toe	25.9	E	.07	.07
Santa Barbara	78-08-13	5.7	885	Goleta UCSB Phys Plant	7.7	A	.39	.24
Santa Barbara	78-08-13	5.7	941	Gibraltar Dam R Abut	18.1	C	.04	.04
Santa Barbara	78-08-13	5.7	5093	Goleta UCSB North Hall	7.7	B	.44	.27
Santa Barbara	78-08-13	5.7	5135	Juncal Dam A	25.4	C	.06	.
Santa Barbara	78-08-13	5.7	5137	Sta Barbara Freitas	10.1	B	.22	.11
Santa Barbara	78-08-13	5.7	9019	Sta Barbara Courthouse	9.8	B	.21	.10
Santa Barbara	78-08-13	5.7	9022	Goleta Substation	11.8	E	.28	.24
Tabas, Iran	78-09-16	7.7	9124	Iran, Tabas	3.0	A	.80	.
Bishop	78-10-04	5.8	1325	Benton Jct 6 + 120	34.2	A	.06	.06
Bishop	78-10-04	5.8	1444	Long Valley Dam	7.6	C	.26	.170
Bishop	78-10-04	5.8	1490	Mammoth Lakes High Sch	29.0	A	.07	.05
Bishop	78-10-04	5.8	9030	Bishop	27.1	A	.06	.03
Malibu	79-01-01	5.0	657	Santa Monica 201 Ocean	20.7	B	.05	.03
Malibu	79-01-01	5.0	757	Sepulveda Control Fac1	26.2	B	.06	.03
Malibu	79-01-01	5.0	5079	Kilpatrick Boys School	20.2	E	.07	.06

APPENDIX
(CONT.)

EARTHQUAKE NAME	DATE YR-MO-DY	MAGNITUDE ^a M	USGS NO.	STATION NAME	FAULT ^b DISTANCE	GEOLOGY ^c CLASS	PEAK GROUND ACCELERATION (g)	
Malibu	79-01-01	5.0	5080	Monte Nido Fire Sta	15.6	C	.06	.05
Malibu	79-01-01	5.0	5081	Topanga Fire Sta	18.1	E	.09	.07
St. Elias, Alaska	79-02-28	7.2	2734	Icy Bay	38.3	A	.16	.11
Coyote Lake	79-08-06	5.9	1251	Corralitos	23.3	C	.03	.
Coyote Lake	79-08-06	5.9	1377	San Juan Bautista	14.4	A	.11	.09
Coyote Lake	79-08-06	5.9	1408	Gilroy Array Sta 1	8.9	C	.13	.10
Coyote Lake	79-08-06	5.9	1409	Gilroy Array Sta 2	8.0	A	.26	.20
Coyote Lake	79-08-06	5.9	1410	Gilroy Array Sta 3	6.3	A	.27	.26
Coyote Lake	79-08-06	5.9	1411	Gilroy Array Sta 4	4.9	A	.26	.24
Coyote Lake	79-08-06	5.9	1413	Gilroy Array Sta 6	4.0	E	.42	.34
Coyote Lake	79-08-06	5.9	1422	Halls Valley	24.8	A	.05	.04
Coyote Lake	79-08-06	5.9	1445	Coyote Creek	3.9	B	.23	.16
Coyote Lake	79-08-06	5.9	1492	San Juan Baut Overpass	16.2	B	.12	.11
Imperial Valley	79-10-15	6.9	117	El Centro Sta 9	5.8	A	.40	.27
Imperial Valley	79-10-15	6.9	286	Superstition Mtn USAF	24.5	D	.21	.12
Imperial Valley	79-10-15	6.9	412	El Centro Sta 10	8.2	A	.23	.20
Imperial Valley	79-10-15	6.9	724	Niland	34.0	A	.10	.074
Imperial Valley	79-10-15	6.9	931	El Centro Sta 12	18.0	A	.15	.11
Imperial Valley	79-10-15	6.9	942	El Centro Sta 6	1.4	A	.72	.45
Imperial Valley	79-10-15	6.9	952	El Centro Sta 5	1.0 ^d	A	.56	.40
Imperial Valley	79-10-15	6.9	955	El Centro Sta 4	4.4	A	.61	.38
Imperial Valley	79-10-15	6.9	958	El Centro Sta 8	3.5	A	.64	.50
Imperial Valley	79-10-15	6.9	5028	El Centro Sta 7	0.2	A	.52	.36
Imperial Valley	79-10-15	6.9	5051	Parachute Test Site	13.1	A	.20	.11
Imperial Valley	79-10-15	6.9	5052	Plaster City	30.5	A	.07	.05
Imperial Valley	79-10-15	6.9	5053	Calexico Fire Station	10.1	A	.28	.22
Imperial Valley	79-10-15	6.9	5054	Bonds Corner	2.8	A	.81	.66
Imperial Valley	79-10-15	6.9	5055	Holtville Post Office	7.3	A	.26	.22
Imperial Valley	79-10-15	6.9	5056	El Centro Sta 1	16.4 ^d	A	.15	.15
Imperial Valley	79-10-15	6.9	5057	El Centro Sta 3	9.3 ^d	A	.27	.22

APPENDIX
(CONT.)

EARTHQUAKE NAME	DATE YR-MO-DY	MAGNITUDE ^a M	USGS NO.	STATION NAME	FAULT ^b DISTANCE	GEOLOGY ^c CLASS	PEAK GROUND ACCELERATION (g)	
Imperial Valley	79-10-15	6.9	5058	EE Centro Sta 11	12.2	A	.38	.38
Imperial Valley	79-10-15	6.9	5059	EE Centro Sta 13	21.5	A	.15	.12
Imperial Valley	79-10-15	6.9	5060	Brawley Airport	7.0	A	.22	.17
Imperial Valley	79-10-15	6.9	5061	Calipatria Fire Sta	22.2	A	.13	.09
Imperial Valley	79-10-15	6.9	5062	Salton Sea	28.0	A	.13	.10
Imperial Valley	79-10-15	6.9	5066	Coachella Canal Sta 4	47.7	A	.14	.11
Imperial Valley	79-10-15	6.9	5090	ICSB	7.0	A	.319	.291
Imperial Valley	79-10-15	6.9	5115	EE Centro Sta 2	10.2 ^d	A	.43	.33
Imperial Valley	79-10-15	6.9	5154	ICSB Free Field	7.0	A	.243	.237
Imperial Valley	79-10-15	6.9	5165	Dogwood Road	4.8	A	.51	.37
Imperial Valley	79-10-15	6.9	9028	Westmoreland Fire Sta	12.6	A	.106	.081
Imperial Valley	79-10-15	6.9	9031	Meloland Ovrps Footing	0.2	A	.326	.279
Imperial Valley	79-10-15	6.9	9032	Meloland Ovrps Abut 1	0.2	A	.408	.264
Imperial Valley	79-10-15	6.9	9033	Meloland Ovrps Abut 3	0.2	A	.359	.303

^a Magnitude (M) selected to be consistent with the moment magnitude scale (see text):

M = M_L for magnitudes less than 6.0
M = M_S for magnitudes 6.0 or greater

^b Fault distance is defined as the shortest distance between the recording station and the fault rupture surface.

^c Geology classification (see Table 2):

A -- Recent Alluvium C -- Soft Rock E -- Shallow Soil
B -- Pleistocene Deposits D -- Hard Rock F -- Soft Soil

^d Consistent with our definition of fault distance, distances were measured from the rupture surface of the Brawley Fault.